UNIVERSIDADE DE LISBOA
FACULDADE DE CIÊNCIAS
DEPARTAMENTO DE ENGENHARIA GEOGRÁFICA, GEOFÍSICA E ENERGIA

The role of wind direction on the occurrence of large fire events in Portugal

Luana Sofia Cardoso dos Santos

Mestrado em Ciências Geofísicas
Especialização em Meteorologia e Oceanografia

Dissertação orientada por:
Carlos Do Carmo De Portugal E Castro Da Camara

2023

Agradecimentos

Quero agradecer a todos aqueles que, de alguma forma, tornaram possível a concretização desta tese.

Em primeiro lugar, quero agradecer ao meu orientador Prof. Carlos da Camara, por ter acreditado em mim e nas minhas capacidades, deixando-me desde cedo fazer parte do seu grupo de trabalho com o qual aprendi o que é fazer investigação em ciência. Agradeço todas as conversas e todos os conselhos que ditaram o rumo deste trabalho, e por todas as vezes que me puxou para cima quando eu me achava perdida. À Sílvia Nunes, por todas as dicas e ajudas fora de horas que me facilitaram e guiaram nesta jornada. A todos os professores da Faculdade de Ciências que fizeram parte do meu percurso académico, por me terem guiado, motivado e contribuindo para o meu enriquecimento científico. À Rute Queiroz por toda a boa disposição e todos os galões com espuma que me serviu.

Obrigado à Ana Marta por todas as conversas e momentos de lazer que me permitiram relaxar nos momentos mais stressantes.

Obrigado ao Miguel Lima, meu companheiro incansável, por ser aquele que está sempre presente e por partilhar todos os altos e baixos desta jornada comigo, um amigo que a faculdade me deu e que com certeza será para toda a vida.

Aos meus pais pelo apoio constante e encorajamento que me têm demonstrado durante todo o meu percurso de vida. Obrigado por me terem proporcionado todas as oportunidades de crescer e alcançar este marco na minha vida académica. Estou eternamente grata por terem acreditado em mim e por terem feito tantos sacrifícios ao longo dos anos.

À minha irmã Iara por sempre me ouvir e aconselhar. Obrigada por estares sempre a meu lado, por todas as palavras de encorajamento e incentivo. És a minha inspiração e os meus exemplos de perseverança e sucesso.

À minha filhota canina Erza, por tornar os meus dias mais preenchidos, de amor e carinho. Obrigada pela tua companhia e travessuras, trouxeste-me o equilíbrio que precisava nesta etapa académica.

A todos os restantes familiares próximos e amigos, obrigado, do fundo do meu coração.

Abstract

Large wildfires have been landmark events in continental Portugal during the last decades, producing catastrophic damages and shaping the socio-economics of the country. In this work, the role of the wind field in wildfires in the last two decades is analyzed to assess the role in triggering or exacerbating these events. Furthermore, this thesis reinforces the need to incorporate information about wind direction in meteorological fire danger indexes.

Two intra-annual peaks of fire activity were found, a mostly human-inflicted smaller peak in March and a major one in the summer period. No significant relation was found between the number of ignitions and burned area, akin to previous studies. Spatially, it was found that ignitions are more frequent in highly populated areas, whereas the larger burned areas are found in the inland, with dense forestation and less population. This discrepancy translates into the fact that only 0.06% of ignitions accounted for nearly 50% of all burned area. The meteorological fire danger, through the Fire Danger Index (FWI), was analyzed per ignition observation, with ignitions which individually originated burned areas above 1000 ha being markedly associated to the conditions of higher fire danger.

Analysis of the wind field in continental Portugal during the warmest period of the year presented a strong northwesterly component while days with more than 1000 ha of burned area, had a prevalence of easterly winds in the ignition points. Principal component analysis was used to identify long shape wildfires, which were furthermore associated with the most intense winds. Considering the wildfires which had their prevalent direction and wind field direction closely aligned (forming an angle less than 45º), they represent 24.2% of all burned area for the 2001-2020 period, although corresponding to only 0.03% of all ignitions. These mostly occur where topography is more complex, in inland Portugal.

Keywords: Wildfires, Wind direction, Fire Danger, FRP, ERA5.

Resumo

O objetivo principal desta tese foi a de avaliar o papel desempenhado pelo campo do vento, nomeadamente a sua direção, em grandes eventos de incêndios em Portugal continental. Os incêndios florestais, nomeadamente os mais catastróficos, são eventos marcantes em Portugal e, nas últimas décadas, vários destes trágicos eventos tiveram fortes impactos na sociedade moldando vários aspetos socioeconómicos e legislativos do país. Este trabalho baseou-se em índices de perigosidade de incêndio, nomeadamente no índice meteorológico de incêndio (Fire Weather Index, FWI) e em dois dos seus sub-índices, os quais foram utilizados para classificar o perigo meteorológico de incêndio no território português através duma análise temporal e espacial no território português. O campo de vento associado aos maiores incêndios florestais das últimas duas décadas foi depois analisado a fim de se avaliar o papel desempenhado pela direção do vento, tanto no desencadear como na intensificação destes eventos, mostrando-se que incêndios com ventos intensos e com direção persistente representam uma percentagem considerável da área ardida em Portugal continental nas duas últimas décadas.

Tal como constatado em estudos anteriores, não foi encontrada uma relação significativa entre o número de ignições e a área ardida, uma característica que se deve ao facto de a existência de maior área ardida depender de fatores tais como condições meteorológicas favoráveis e combustível disponível para impulsionar e alimentar o fogo, além de uma ignição para gerar o mesmo. Foram identificadas três grandes épocas de incêndio no período que cobre 2001-2020, em 2003, 2005 e 2017, sendo o primeiro e último os episódios com maior área ardida e o intermédio aquele que apresenta o maior número de ignições. A variabilidade mensal relacionada com fogos (ignições e área ardida) apresenta dois picos, um maior e um secundário: o menor deles, que ocorre no mês de março, está relacionado com as queimadas controladas provocadas pelo homem em regiões agrícolas; o maior pico, que se estende por julho, agosto e setembro, corresponde ao período de verão tipicamente mais quente e seco. O estudo foi ainda efetuado através da análise de gráficos espaciais de estimativas de densidade kernel (Kernel Density Estimation, KDE), que revelam que o número de ignições se concentra maioritariamente junto dos maiores centros populacionais do Porto, Baixo Minho e Lisboa. Por outro lado, a maior área ardida é observada numa área de menor densidade populacional e em regiões altamente florestadas nas regiões da Beira e do Algarve. Esta discrepância entre as áreas prevalentes de ignições e a área ardida deve-se ao facto das zonas de maior densidade populacional terem mais vigilância, ao invés das menos povoadas, além de que estas zonas têm também mais terrenos não conservados, i.e., com menor manutenção, o que leva a uma maior disponibilidade de combustível para a progressão dos incêndios. A este respeito, no período 2001-2020, cerca de 0.10 % das ignições (que corresponde a 426) excederam 1 000 ha de área ardida, sendo que 60 % destas (que corresponde a 266 ou 0.06 % do total) representaram quase 50 % de toda a área ardida em Portugal continental.

A distribuição geográfica do FWI apresenta um gradiente noroeste-sudeste com os seus valores a aumentar em direção ao sul do território. Esta distribuição está relacionada com a climatologia do país, sendo o norte mais húmido enquanto o sul é árido com temperaturas mais elevadas. Dois sub-índices, o índice de propagação inicial (Initial Spread Index, ISI) e o índice de combustível disponível (Buildup Index, BUI), que compõem o FWI, foram analisados individualmente, apresentando uma disposição geográfica semelhante ao FWI. Observou-se que essas três variáveis apresentaram valores mais elevados no verão, nos meses de junho, julho e agosto. Tanto o ISI como o BUI apresentam evoluções diferentes em função das características que lhes são inerentes, sendo que o primeiro evolui suavemente ao longo do ano enquanto o segundo cresce até ao final do verão, altura em que apresenta um decréscimo abrupto no início do outono, principalmente devido a um aumento da humidade nesta altura do ano.

Consequentemente, o FWI segue estas distribuições, com valores medianos no verão em torno dos 25 e valores extremos que atingem o máximo em torno dos 40. Para além disso, analisou-se a relação destas três variáveis por observação de ignição, sendo que o grupo de ignições superiores a 1 000 ha representa de forma notável as condições de maior perigo de incêndio, com valores dos três índices analisados mais elevados.

A análise do campo de ventos em Portugal continental mostrou que existe um ciclo anual bem definido. Nos meses de inverno (definido de novembro até fevereiro), a circulação é predominantemente de leste, sudeste e sul, enquanto nos meses mais quentes, entre maio e setembro, apresentam uma forte componente de noroeste. Nos dias que ultrapassaram os 1 000 ha ardidos, os pixéis que registaram ignições entre 2001 e 2020, no período de verão prolongado, apresentaram uma prevalência de ventos de leste, em contraste com a circulação predominante neste período do ano. Selecionou-se uma amostra de 266 incêndios florestais associados a uma área ardida superior a 1 000 ha, representando cerca de 50 % da área ardida em 2001-2020 e, através de análise de componentes principais (Principal Component Analysis, PCA), 208 eventos foram classificados como incêndios florestais de forma alongada (aqueles cuja primeira componente principal explicava mais de 70 % da variância espacial total da cicatriz). Utilizou-se, em seguida, um filtro que reteve 152 eventos em que a média vetorial dos ventos com intensidade igual ou superior ao percentil 75 era superior a 10 km/h. Finalmente, constituiu-se um subconjunto de fogos alinhados restringindo os fogos em que o ângulo entre a direção da primeira Componente Principal e a direção do vento médio era inferior a 45 º. Estes incêndios alinhados, que representam 24.2 % de toda a área ardida no período 2001-2020 em Portugal Continental, ocorreram maioritariamente no centro do território, onde a topografia é mais complexa com extensas cadeias montanhosas que possuem um coberto florestas e vegetal considerável, e o campo de vento a eles associado apresentou uma maior componente de noroeste e de sul, coincidindo com a orientação das áreas florestais aí presentes.

Este trabalho destaca a importância do papel desempenhado pelo vento, nomeadamente a sua direção, nos grandes eventos de incêndio em Portugal e salienta que os incêndios florestais não estão diretamente ligados a um único tipo de direção do vento, mas também à localização geográfica onde ocorrem. Assim, tendo em conta que uma pequena parte das ignições filtradas, representando apenas 0.03 % do total de ignições, englobam uma área ardida estendida e alinhada com um campo do vento intenso, responsável por uma parte substancial da área ardida, que representa 24.2 % do total de área ardida. Se a direção do vento for a adequada (e se todas as outras condições, nomeadamente a presença de combustível, tiverem lugar), uma pequena ignição pode transformar-se num grande incêndio de forma descontrolada e dificultando o seu combate e gerência. É, portanto, de grande interesse considerar a direção do vento ao analisar índices de perigo de incêndio como o FWI pelo que há vantagens em incorporar esta variável nas avaliações de perigo de incêndio, bem como a consideração do tipo de vegetação integrada com a direção do vento, uma vez que é preponderante na evolução do fogo.

Palavras-chave: Grandes fogos, Direção do vento, Perigo de incêndio, Potência radiativa de fogo, ERA5.

Contents

List of Acronyms and Abbreviations

BUI	Buildup Index
CFFWIS	Canadian Forest Fire Weather Index System
COS	Carta de Ocupação do Solo
DC	Drought Code
DGT	Direção Geral do Território
DMC	Duff Moisture Code
E	East/Easterly
ECMWF	European Centre for Medium Range Weather Forecasts
ERA5	Fifth generation ECMWF reanalysis
ETRS89	European Terrestrial Reference System 1989
FFDRS	Forest Fire Danger Rating System
FFMC	Fine Fuel Moisture Code
FRP	Fire Radiative Power
FWI	Fire Weather Index
FWIe	Enhanced Fire Weather Index
ICNF	Instituto da Conservação da Natureza e das Florestas
ISI	Initial Spread Index
JJA	Warmer months
JJASO	Months of the extended summer period
KDE	Kernel Density Estimation
LULC	Land Use Land Cover
MMU	Minimum Mapping Unit
N	North/Northerly
NAO	North Atlantic Oscillation
NE	Northeast/Northeasterly

NW	Northwest/Northwesterly
PC	Principal Component
PCA	Principal Component Analysis
RH	Relative Humidity
S	South/Southerly
SE	Southeast/Southeasterly
SGIF	Sistema de Gestão de Informação de Incêndios Florestais
SW	Southwest/Southwesterly
U/V	Zonal/Meridional wind component
UTC	Universal Time Coordinated
X/Y	Cartesian position
W	West/Westerly
WGS84	World Geodetic System 1984

List of Figures

List of Tables

Chapter 1 Introduction

1.1 Initial considerations

Wildfire is a natural phenomenon that affects many ecosystems worldwide. While some forest ecosystems may benefit from fires acting as population control (Pausas and Keeley, 2019), these events often pose a substantial risk to the balance of the ecosystems (Amatulli et al., 2013; Amraoui et al., 2015; Fernandes et al., 2016). Additionally, wildfires often constitute a danger for humans, causing socio-economic damage, injuries, and deaths. Wildfire events greatly depend on ignition factors, topography, land cover, forest fire management and suppression policies, and weather conditions (Amatulli et al., 2013; Carmo et al., 2021; DaCamara et al., 2014; Trigo et al., 2006a).

The distribution of wildfires is worldwide (Figure 1.1). The most affected continent is Africa, namely the tropical areas closer to the Equator. South America, southwest Russia and southeast Asia also present a high number of wildfire events. In the last 20 years, the regions that produced the most catastrophic fires (overall size and rate of spread) were the African southern tropical band, northern Australia, the boreal forests in Canada, Alaska, and Russia, and Mediterranean climate areas such as Portugal, Greece, Turkey, California, and Chile (Artés et al., 2019).

Regarding Mediterranean Europe, when considering the southern European countries with largest portion of burned area (Portugal, Spain, France, Italy, and Greece), Portugal has been hit in the last decades by several catastrophic fire seasons (Figure 1.1a), associated to tragic episodes (Pinto et al. 2018b; San-Miguel-Ayanz et al., 2021). Table 1.1 shows the number of ignitions and amount of burned area in the aforementioned countries, and it is worth emphasizing that Portugal was the country that contributed the most in both number of ignitions, with 490 980 (46.7% of the total amount), and burned area, with 3 057 864 ha (38.3% of the total burned). Due to the prevalence of large and intense wildfires, this area has been the subject of several studies at Instituto Dom Luiz (DaCamara et al., 2014; Nunes et al. 2019; Pinto et al. 2018a; Trigo et al., 2006a).

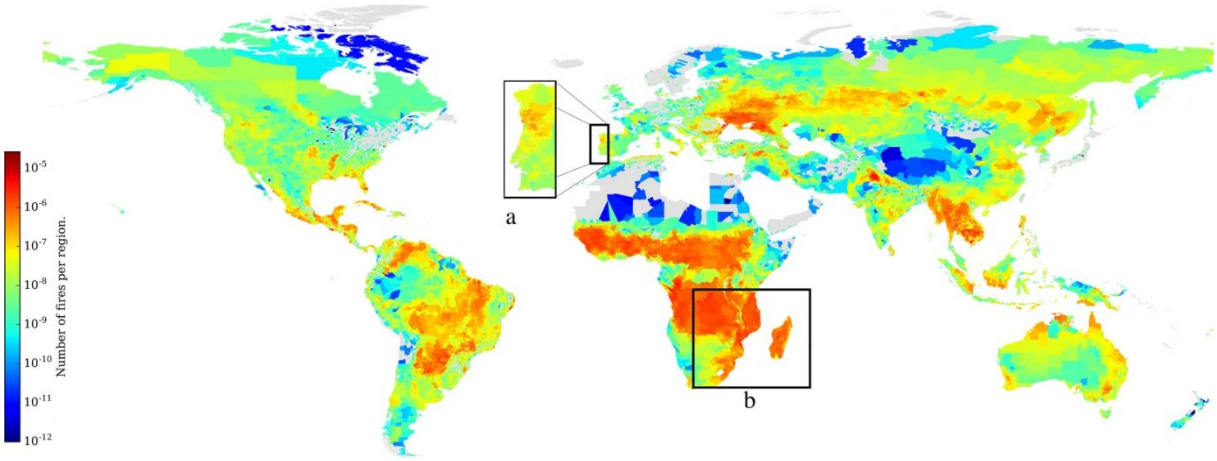

Figure 1.1 – Number of fires per region surface from 2001 to 2017. Source: Artés et al., 2019.

Table 1.1 – Cumulative number of ignitions and burnt area (hectares) in five Southern Member States for the 2000-2020 period. Adapted from San-Miguel-Ayanz et al., 2021.

	Portugal	Spain	France	Italy	Greece	Total
Number of Ignitions	**490980 (46.7)**	310030 (29.5)	90204 (8.6)	131648 (12.5)	27463 (2.6)	1050325
Burned Area [ha]	**3057864 (38.3)**	2283353 (28.6)	365452 (4.6)	1533509 (19.2)	743880 (9.3)	7984058

An important framework when studying fire behavior is the triangle of fire (Moritz et al., 2005; Bickerton, 2012), which can be conceived at different scales in space and time (Figure 1.2). At the smallest scale, each of the vertices of the triangle is crucial for fire development: heat, fuel, and oxygen. The first component, heat, is the source of energy that starts the fire, raising the temperature of the fuel (wood, paper, oil, etc.) up to the ignition point; once this is achieved, the fuel will begin to break in a chemical reaction that requires oxygen (combustion). When any of these three elements, heat, fuel and oxygen are removed from the fire triangle, fire cannot take place. Firefighters use this rationale to control or put out wildfires by removing either one or more of these components. Furthermore, this concept is important to minimize the potential danger for wildfire occurrences, since the reduction of both heat sources (chiefly human induced ignitions in Mediterranean Europe) and fuel (mainly wildland cleaning and management) have critical roles (Syphard & Keeley, 2015). Regarding the heat sources, it is observed that about 95 % of wildfires were initiated through human-caused ignitions, either negligent or intentional, over areas in California and the Mediterranean basin (Leone et al., 2009; Goméz-Gonzaléz et al., 2018), regions that have been substantially affected in the last decades.

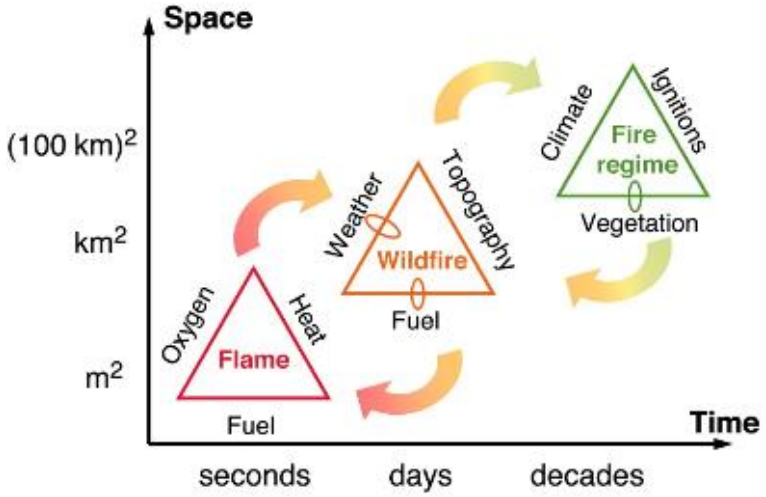

Figure 1.2 – Controls on fire at different scales. Dominant factors that influence fire at the scale of a flame, a single wildfire, and a fire regime. Retrieved from Moritz et al., 2005.

1.2 Mediterranean region, climate, and wildfires

The Mediterranean region is characterized by warm, dry summers and mild, wet winters (Lionello et al., 2006). The climate affecting this area, the so-called Mediterranean climate also affects other areas around the globe such as California, Chile, or Australia (Di Castri, 1991). The Mediterranean climate

has a significant impact on the landscape, flora, and fauna of the regions. Furthermore, southern European climate is heavily regulated by the western oceanic circulation. This circulation can be disturbed by the meandering and wave breaking cycles of the jet stream, which can lead to both periods of quasi-stationary high-pressure systems and transient cyclonic systems. Both these events lead to differing impacts that can modulate southwestern Europe's, and particularly Iberia's climate (Lionello et al., 2006; Santos & Corte-Real, 2006). In the summer months, high-pressure systems related to atmospheric blockings and subtropical ridges have a substantial influence in regulating Iberian climate, deflecting smaller cyclonic systems that are favorable for clouds and storms, generally leading to a sunny and dry environment. Thus, there is a positive influence in the temperature created by radiative imbalance, namely in the interior of the Peninsula; additionally, the dry warm advection from these areas further influences other regions near these high-pressure areas, such as the southwestern coasts (Sousa et al., 2018). In contrast, the winter months are mild and wet. This is due to the influence of moist air from the Atlantic Ocean, which blows into the region, resulting in milder temperatures, and abundant rainfall that is critical for the growth and survival of the region's vegetation (Lionello et al., 2006).

In short, the weather circulation over the Iberian Peninsula is mostly related to two large drivers, the Azores High, and the North Atlantic Oscillation (NAO) (Cresswell-Clay et al., 2022; Trigo et al., 2006b). The first driver, the Azores High, is a semi-permanent atmospheric high-pressure system that originates over the Atlantic Ocean. This system influences the sub-tropical latitudes in western Europe and may prevent Atlantic low-pressure systems from reaching western Europe. Its influence is further exacerbated in the Iberian Peninsula since its movement over from the northern Atlantic towards Europe may contribute to the transport of warm and drier air from northern Africa contributing to hot and dry summers (Cresswell-Clay et al., 2022). In contrast, the Azores High also acts as a barrier, preventing the influence of Atlantic low-pressure systems evolving towards this area, leading to clear and sunny weather year-round. The second driver, NAO, a large-scale fluctuation in the atmospheric pressure difference between the middle and the subpolar latitudes in the Atlantic, presents two phases. Positive NAO phases are characterized by lower pressure in the north (around Iceland) and higher in the south (around Azores), leading to cold and dry conditions in the Iberian Peninsula. On the other hand, negative NAO phases (reverse pattern), lead to warm and wet weather in the region (Rodrigo, 2021; Trigo et al., 2006b).

In recent years, and most prevalently in the last two decades, the Iberian Peninsula has been impacted by multiple severe wildfires. These events are getting more catastrophic, that are partly attributable to periods of drought, and to intense heatwaves that have been exacerbated by climate change (García-Herrera et al., 2019; Kautz et al., 2022). Additionally, the expansion of urban areas, the decrease in agricultural fields and increase of shrubland and forest have dramatically changed the landscape, increasing the risk of wildfire. The impact of wildfires in the peninsula can be devastating, harming both the environment and local communities, with damages ranging from the destruction of habitat, disruption of wildlife, soil erosion, and release of pollutants into the air and water; with all producing a combined effect on health of humans and animals, as well strain the economic system (Abatzoglou et al., 2019; Pereira et al., 2013).

Relating the previously mentioned concepts of the fire triangle (Figure 1.2) and the typical climate of Iberia, there are areas where the danger of wildfire is higher. This essentially occurs in central, and northern Portugal, and northern Spain (as shown in the zoomed area in Figure 1.1), mostly forested areas which, in case of vegetation stress due to prolonged droughts and heatwaves, can lead to extreme potential fire danger (Ermitão et al., 2022; Ribeiro et al., 2020). Complementing the concept of the fire triangle, looking at different scales (Figure 1.2), there are several other factors that influence fire behavior and relate directly with these areas in Iberia, such as the already mentioned fuel, weather,

climate, ignitions, and vegetation. Another crucial factor is topography, which is very complex in central and northern Iberia, with peaks exceeding 2 000 m and prevalence of mountain systems over most of the territory in the north. Critically, this conditions fire evolution, that directly involve both topography and the atmospheric flow over mountain slopes, generally associated to higher atmospheric instability (Alcubierre et al., 2011; Lecina-Diaz et al., 2014).

The 2017 fire season in Portugal, where a large area of the territory burned (more than 500 000 ha), was especially tragic, causing widespread damage and substantial loss of life. This season was mostly divided into two major episodes, the first one in June and the second in the month of October, typically outside the critical period of the year. These events claimed the lives of more than 100 people and prompted authorities from both countries to implement measures that aimed at preventing occurrences when high danger is verified (Pinto et al., 2018b). To mitigate the risk of wildfires in this region, it is important to take a multi-disciplinary approach, incorporating measures to prevent fires, improve fire response, and manage the landscape. This includes implementing fire-resistant land use planning, reducing fuel loads through controlled burns and vegetation management, and improving fire response and suppression capabilities, as well as investing in educating the population, mainly rural, on the issue.

In short, the relationship between the Iberian climate and wildfires is complex and multifaceted. The hot and dry weather conditions in the region, combined with human activities and land usage, have increased the risk of wildfires in the Iberian Peninsula (DaCamara et al., 2014; Nunes et al. 2019; Pinto et al. 2018a; Trigo et al., 2006a). It is therefore crucial to take a proactive approach when addressing the issue of reducing the risk of wildfires in the region.

1.3 Meteorological fire danger

Fire danger ratings have been used since the middle of the last century to better assess the current and near-future meteorological, hydrological, and vegetation conditions that could contribute to fire spread or fire intensity. Some of these indexes were built taking into account regional conditions, e.g. the Canadian Forest Fire Weather Index System (CFFWIS) that was developed for the Canadian boreal forests (van Wagner, 1987), the McArthur's Forest Fire Danger Rating System (FFDRS) for Australia (Dowdy et al., 2009), and the Nesterov ignition index for Central and Eastern Europe and Siberia (Stocks et al., 1996).

All above-mentioned indexes consider meteorological variables such as wind intensity, dew and absolute temperatures, relative humidity or precipitation, and with different levels of relative importance, they include memory components for humidity of the fuel or soil, to assess fuel stress (Dowdy et al., 2009; Stocks et al., 1996; van Wagner, 1987). CFFWIS's Fire Weather Index (FWI) has been successfully used in the past decades in several areas of the world affected by wildfire such as southeast Asia (de Groot et al., 2007), New Zealand (Alexander, 1994), or Mediterranean Europe (DaCamara et al., 2014; Pinto et al., 2018a).

This meteorological fire danger index system, CFFWIS, is composed of six different indices (van Wagner, 1987), three fuel moisture codes with a memory component (the Fine Fuel Moisture Code; the Duff Moisture Code; and the Drought Code), and two fire behavior indices based on the aforementioned codes and wind intensity (the Initial Spread Index; the Build-Up Index). The two latter indexes are combined into FWI, which stands for a numeric rating of fire intensity that gives an idea of the meteorological fire danger. In Iberia, FWI presents higher values in the south than in the north that are mainly due to the contrast in temperature, and lower values near the ocean and mountainous areas.

Pinto et al. (2020) added a new component to the traditional FWI, accounting for atmospheric instability, thus resulting in an enhanced FWI (FWIe). This novel index aims at representing an increased danger induced by high instability situations in the lower troposphere. Following that study, Santos et al. (2023) performed the first climatological and evolution analysis of these indexes for the 1980-2020 period. Both FWI and FWIe have been observed to be increasing in the Iberian Peninsula during summer. Lacking in these indexes, however, is a term accounting for the directionality of wind, which in some cases is crucial when there is a marked landscape orientation.

1.4 Large wildfires in Portugal and the main causes

Portugal is one of the territories that is most affected by wildfires in Europe. Since 1980, when official fire records started, there has been several important fire seasons (San-Miguel-Ayanz et al., 2021), with 2005 and 2017 standing out being as the most catastrophic, the first one with more than 330 000 ha of burned area (Martins et al., 2012) and the second one with more than 500 000 ha (Ermitão et al., 2022). Both years showed exceptional extreme fire conditions, and the most intense droughts on record. The first extended from the 2004 fire season to 2005, and affected most of southwestern Europe, while the second exceeded it, affecting most of the continent over the 2016-17 years (García-Herrera et al., 2019).

The 2017 season was affected by two mega-episodes, each with over 200 000 ha burned due to somewhat different circumstances (Pinto et al., 2018b). First during the month of June and July, in the beginning of the fire season, both fire danger and atmospheric instability were high which, coupled with a heat wave and drought conditions increased the fuel available to burn and the potential for fire spreading (Ermitão et al., 2022). Later, in October, the close passage of Hurricane Ophelia advected warm and dry air from northern Africa as well as increased the wind field intensity in continental Portugal, producing an exceptional situation for fire occurrence which is rather odd at this time of the year (Pinto et al., 2018b). Overall, the 2017 fire season saw the tragic passing of 116 people and nearly 300 injuries, with incalculable socio-economic and biological losses.

1.5 Motivation and thesis structure

Freire and DaCamara (2019) developed a model (cellular automaton) designed to simulate a severe wildfire episode that took place in Algarve (southern Portugal) in July 2012. This model was developed to respond to wind-driven wildfires by introducing a wind propagation rule in which fire is allowed to spread to nonadjacent cells placed along the wind direction. Following that study, the same model was applied to two singular cases during the 2017 October wildfires, and it was observed that model simulations with different inputs of wind direction resulted in very different values of probability for the area to burn (Mota et al., 2022). This analysis is particularly relevant since this episode occurred with intense southern circulation, resulting in several wildfires following this prevalent direction. Additionally, the land cover in which the wildfire is inserted is also important, not just the type but also the distribution. In October 2017, it was observed that some of the largest wildfires spread along land covers with north-south directionality (Figure 1.3).

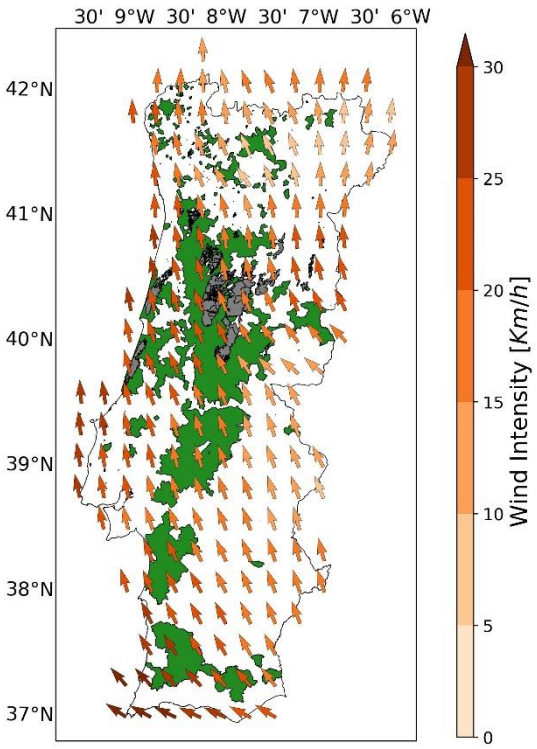

Figure 1.3 – October 15th, 2017, fires in mainland Portugal. Forest regions from COS2018 are presented in green. 10 m wind field is presented by the orange quivers with the associated intensity shown in the color bar. Burned areas from the wildfires that started on this day are represented by grey shapes.

This suggests to better understanding the role of wind direction and its relation to the environment relative to wildfire propagation. This thesis aims to assess the role played by wind direction in the large wildfires that affected Portugal in the past decades. Furthermore, this analysis pretends to relate the prevalent circulation direction with the landscape orientation. This work is structured in 4 chapters, the present one providing a general background on wildfires and the scope of the thesis, followed by a chapter explaining the approach adopted in this study, and a third one describing the results obtained. The thesis ends with a chapter presenting the main findings of this work.

Chapter 2 Data and Methodology

The present study focusses on mainland Portugal and spans the 1980-2020 period. The analysis relies on multiple data such as meteorological fields, land cover information, ignition and hotspot records and burned area scars. Several methods were used to analyze the data, which will be described in the following subsections.

2.1 Data

2.1.1 Canadian Forest Fire Weather Index (FWI) System

The Canadian Forest Fire Weather Index (FWI) is a weather-based index used to rate the potential for wildfire conditions. This index was initially used for Canadian forests and its operational application was popularized in the 1970s (Wang et al., 2015). Its calculation depends on daily inputs, at local noon, of surface absolute temperature, surface relative humidity (RH), near-surface wind speed, and 24 hour accumulated precipitation.

The system is made up of six different indices (Figure 2.1) which are divided into two main categories: the fuel moisture codes and the fire behavior indices. The first ones are the Fine Fuel Moisture Code (FFMC), Duff Moisture Code (DMC), and Drought Code (DC), and these possess a memory component to assess the moisture content at different depths of the soil. The second ones are the Initial Spread Index (ISI), the Build Up Index (BUI) and the Fire Weather Index (FWI). ISI combines FFMC with wind speed and provides the rate at which a fire will spread when the fine fuel is dry without the influence of the deeper soil condition. On the other hand, BUI combines DMC with DC to represent the total fuel available to the spreading of a fire. While ISI provides a measure of how quickly a fire can spread BUI gives a rate of fire intensity potential. BUI and ISI are finally combined into FWI that evaluates the intensity of a fire in the case of an ignition. For more detailed information about this fire danger index and its construction it is advisable to visit Van Wagner (1987).

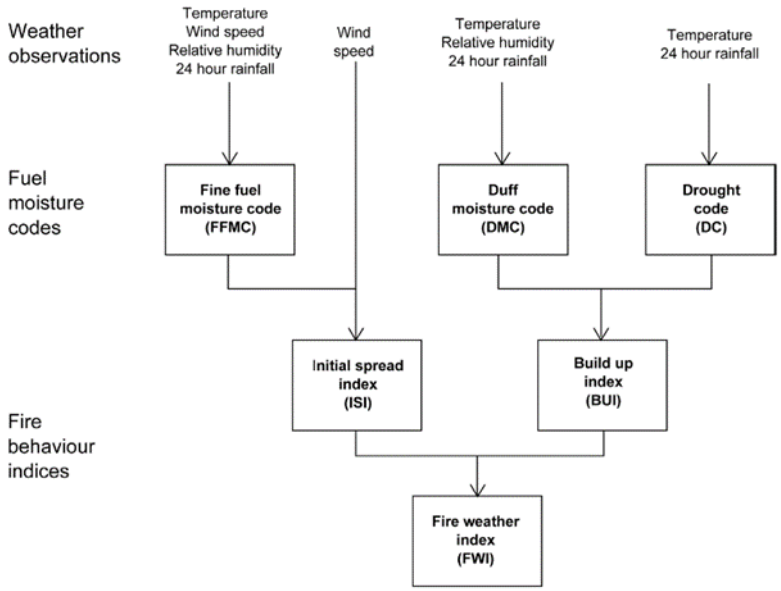

Figure 2.1 – Fire Weather Index calculation scheme. Source: Lehtonen et al., 2014.

All indices were computed relying on a source-code available at Wang et al. (2015) and using meteorological data retrieved from ECMWF's fifth generation reanalysis, ERA5.

2.1.2 Reanalysis data

To evaluate the wind direction at the surface and to calculate the previously discussed fire danger indices, meteorological data were retrieved from the fifth generation of the European Centre for Medium Range Weather Forecasts (ECMWF) global reanalysis (ERA5, Hersbach et al., 2020). The data is available worldwide in a 0.25°x0.25° spatial grid and for this study, it was accessed data over the mainland Portugal region from 1980 to 2020. For this study the following data was retrieved: zonal and meridional wind components (U and V, respectively) at 10 m, temperature and dew point temperature at 2m, and 24 hour accumulated precipitation. In the indices computation all fields refer to 12 UTC.

Since the ERA5 reanalysis data set only provides surface dew point temperatures it was necessary to apply the Magnus relation which yields a conversion between relative humidity and dew point temperature with a relative error inferior to 0.4% over the range -40°C ≤ T ≤ 50°C (Lawrence, 2005):

$$T_d = \frac{B_1\left[ln\left(\frac{RH}{100}\right) + \frac{A_1 T}{B_1 T}\right]}{A_1 - ln\left(\frac{RH}{100}\right) - \frac{A_1 T}{B_1 + T}} \quad (2.2.1)$$

where $A_1 = 17.625$ and $B_1 = 243.04°C$ are the conversion coefficients.

Consequently, the computation of RH can be easily derived from equation (2.2.1), this time depending on the dew point temperature:

$$RH = exp\left[\left(\frac{A_1 B_1 (T_d - T)}{(B_1 + T_d)(B_1 + T)}\right)\right] \times 100 \quad (2.2.2)$$

Applying the later conversion (2.2.2) to the 2m dew point temperature we obtain 2m relative humidity, the last ingredient from the 4 to compute the fire danger indexes.

Hereafter, the wind direction, retrieved from both the U and V wind components at 10m, is taken as the meteorological wind direction and this computation was made according to ECMWF, 2022. In this system, the wind direction increases clockwise starting at 0° as a northerly wind, 90° as an easterly wind, 180° as a southerly wind, and 270° as a westerly wind.

2.1.3 Fire database

Information about ignitions that occurred in mainland Portugal were retrieved from the Portuguese database from "Instituto da Conservação da Natureza e das Florestas" (ICNF, https://www.icnf.pt/). Data for the 2001-2020 period were processed by the Portuguese "Sistema de Gestão de Informação de Incêndios Florestais" (SGIF) and contains, among other information, start and end dates of fire episodes, the latitude and longitude of the ignition point and the total burned area (in hectares). In this study we restricted events with more than 1 000 ha of burned area.

2.1.4 Burned area scars

Burned area scars were also provided by the Portuguese "Instituto da Conservação da Natureza e das Florestas" (ICNF, https://geocatalogo.icnf.pt/). This data set allows identifying the area affected by wildfire events that occurred from 1975 to 2020 in ETRS89/PT-TM06 cartographic coordinate system.

From 2013 onward, the data set includes information about the start and end dates of most burned scars. Previously to 2013, some of the largest burned scars are related to different fires ignitions and, for those cases, a visual analysis, using information about Fire Radiative Power (FRP), was conducted in order to delimit the scars associated to the different fire ignitions.

2.1.5 Fire Radiative Power (FRP)

Fire Radiative Power (FRP) that represents the power released by a given identified hotspot was retrieved from the MODIS Collection 6 Active Fire Product (Giglio et al., 2018) available from 2001 to 2020 (https://earthdata.nasa.gov). The data set provides for each hotspot the latitude and longitude, date and time, fire confidence, fire radiative power (expressed in megawatts) and type of hotspot (i.e., presumed vegetation fire, active volcano, other static land source or offshore). In this study, selected FRP data were restricted to presumed vegetation fire events with fire confidence greater than 90 %.

2.1.6 Land cover and population density

Forest and shrub coverage information was retrieved from the Portuguese "Carta de Ocupação do Solo" (COS) produced by Direção Geral do Território – DGT (https://snig.dgterritorio.gov.pt/), available for 2018. Data consist in polygons with a Minimum Mapping Unit (MMU) of 1 ha and 83 classes of Land Use Land Cover (LULC) of which 11 are attributed to the forest and shrub class (Direção-Geral do Território, 2019). In this study, only parishes with more than 55 % of its area identified as forest and/or shrub were considered to create the forested region map for mainland Portugal.

The population density data (in number of inhabitants per square kilometer) is available from the PORDATA website (https://www.pordata.pt/) [1], which provides useful information for Portugal and Europe. Data consist of annual estimations, at a county scale, for 2001 and for 2009 to 2020 period, and was used to compare the geographical distribution of the Portuguese population with those of ignitions and burned areas.

2.2 Methodology

2.2.1 Principal Component Analysis

In order to study the relation between wind direction and fire propagation, it was necessary to explore whether burned scars had a preferential direction of propagation. Thus, Principal Component Analysis (PCA) was used (Jolliffle, 2002) to the burned areas to determine that preferential orientation and its contribution to the shape of the scar.

For each burned scar, Principal Component was applied to the ETRS/PT-TM06 (X,Y) coordinates which allows to conserve distances instead of areas, leading to two Principal Components (PCs) that are orthogonal, and therefore the total variance of the coordinates is equal to the summation of the variance of each PC. Accordingly, the more variance explained by PC1 (the component with largest variance), the more elongated the burned scar along the direction defined by this PC (Figure 2.2). Principal components for selected burned scars were computed according to Tipping & Bishop (1999), through

[1] More information on this data can be found in PORDATA

the scikit-learn.org Python package. For representation purposes, a projection to WGS84 was made, the same as the FRP, using ArcMap10.8.1 projection tools.

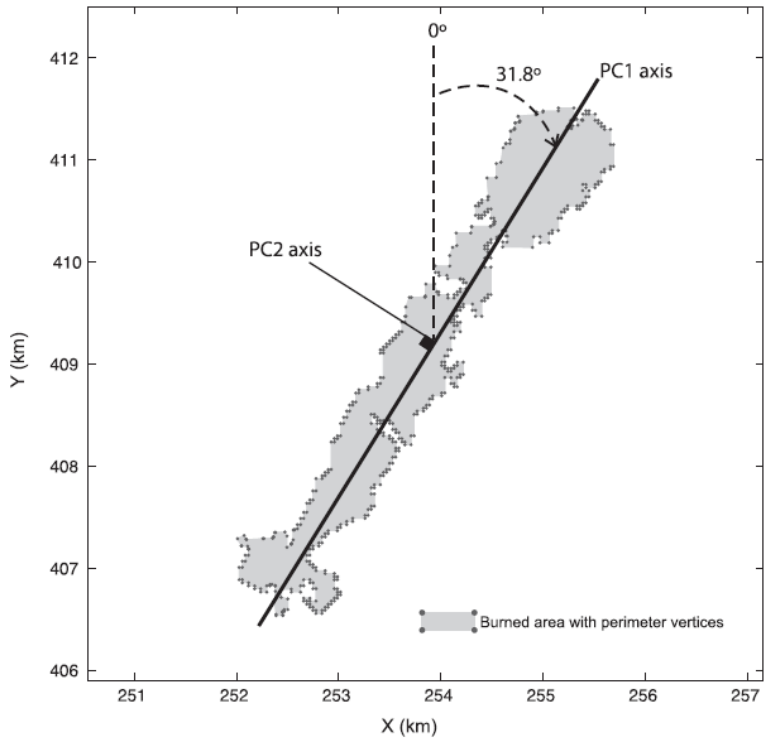

Figure 2.2 – An example of results obtained when applying PCA to a scar. Source: Barros et al., 2011.

2.2.2 Kernel Density Estimation (KDE)

To analyze the spatial distribution of wildfire occurrences, a kernel density estimation (KDE) was performed. The analysis consists in smoothing a 2D histogram over a chosen geographical area. This is achieved using a Gaussian kernel which produces a smooth and continuous distribution of probabilities over a two-dimensional grid (Fotheringham et al., 2000).

Chapter 3 Results

3.1 Characteristics of wildfires

For the 2001-2020 period, 456 842 fires were observed in continental Portugal, with 426 of those corresponding to ignitions that resulted in over 1 000 ha of burned area, around 0.10 % of all events (Table 3.1). The number of ignitions resulted in a total amount of nearly 3 million ha of burned area, from which the subset of ignitions originating burned areas larger than 1 000 ha contributed to over 50 % of burned area, meaning that only 0.10 % of ignitions were responsible for more than 50 % of the total burned area in the last two decades.

Table 3.1 – Distribution of occurrences within this study. The first column indicates the types, the second the number of events, and the third the corresponding burned area.

	Number of events	**Burned area [ha]**
Total ignitions	456842	2 898 245.7
Ignitions above 1000 ha	426 (0.10% of total)	1 559 161.1 (53.8%)

Figure 3.1 shows the inter-annual distribution of the number of ignitions (in orange) compared to the value of burned area (in grey) for the same period of 2001-2020. The number of ignitions that originated more than 1 000 ha of burned area is shown above the bar corresponding to the total number of ignitions (Figure 3.1, orange bars). Additionally, the grey bars are divided into two parts, with the dark tone corresponding to the burned area of ignitions originating more than 1 000 ha, with the equivalent percentage being shown at the top. Here, three years can be highlighted: 2003, 2005, and 2017, since these years reached national records of burned area (2003 and 2017) and ignitions (2005). In 2003, 21 people perished and more than 1 000 M € in damages were registered; in 2005 12 fire-fighters died; and finally, the 2017 fire season was the most severe with the passing of 116 citizens and serious impacts at social, economic, and ecological levels (Schmuck et al., 2004; Schmuck et al., 2006; Pinto et al., 2018b). A special feature of these three years is that neither 2003 nor 2017 had the greatest number of ignitions in the last 40 years (10th and 20th greatest, respectively), while having the second and the first largest burned areas, respectively, which had a high contribution of those ignitions above 1 000 ha (79 % and 82 % of the burned area in those years, respectively). On the other hand, it can be seen many years exceeding the number of ignitions to those seen in 2003 (Figure 3.1 shows the last 20 years) with a small portion of burned area. This representation shows the lack of relation between both variables as already mentioned in the *Introduction* section, since the probability of higher burned area is dependent on factors such as favorable weather conditions, available fuel to burn, besides an ignition to generate fire; an analogy to the triangle of fire (Moritz et al., 2005) previously discussed (Figure 1.2).

The annual cycle of number of ignitions and cumulated burned areas is presented in Figure 3.2 using the same conventions of Figure 3.1. Two peaks are conspicuous in the cycle, for both ignitions and burned area, a secondary one centered in the month of March which is mainly due to controlled burning by humans (thus leading to a larger number of ignitions with a smaller burned area), as referred in the *Introduction* section. The main peak is centered in the months of July, August and September and is about 4.5 times larger than the March one regarding the ignitions (and with a larger difference for burned area, since the March peak is more subtle). This corresponds to the summer-period related wildfires, as can be verified by the higher values of burned area (Figure 3.2). Here, the period compromised by the months of June, July, August, September, and October (JJASO) is referred to as the extended summer, since it has the greatest fire activity (ignitions and burned area), and it is expected that the duration of

the fire season will increase with climate change (Pereira et al., 2013). Furthermore, a noticeable partition of burned area caused by those ignitions above 1 000 ha is seen during the months of July, August and most noticeable in October, the later one corresponding to the catastrophic 2017 Portuguese October wildfires (providing for 69 pp of the 71%) which contributed alone to over 200 000 ha burned in just a 24-hour period.

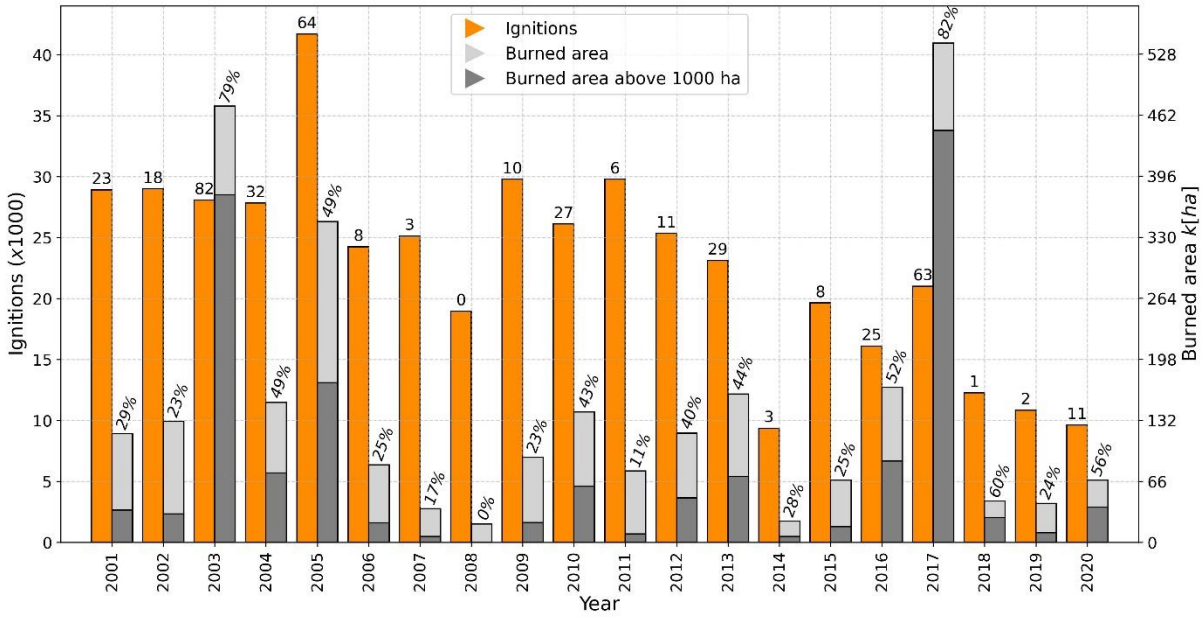

Figure 3.1 – Inter-annual distribution of the number of ignitions (orange) and burned area (grey) in Portugal, for the 2001-2020 period. Number of ignitions that exceeded the 1 000 ha of burned area is shown above the number of ignitions bar (orange). Grey bars are divided in two, with the dark tone corresponding to the burned area of those ignitions that exceeded 1 000 ha, with the equivalent percentage being shown at the top.

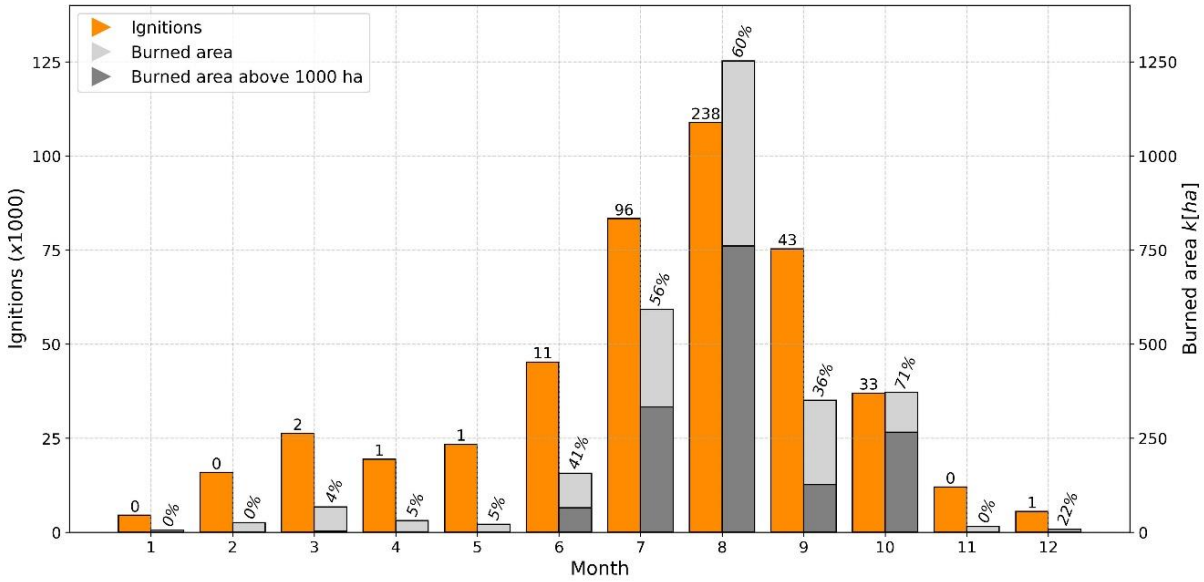

Figure 3.2 – Monthly variability of the cumulative number of ignitions (orange) and cumulated burned area (grey) in Portugal, for the 2001-2020 period. Numbers and partition of gray bar same as Figure 3.1.

For a better comprehension of the heterogeneities between the number of ignitions and cumulated burned area, spatial KDE plots were produced with the geographical distributions (Figure 3.3), considering the period between 2001-2020. First, the geographical distribution of the number of

ignitions (Figure 3.3A) shows great zonal and meridional contrasts, a primary focus around the Porto, Guimarães and Braga regions and a second one in the Lisbon region. This resembles the population density distribution as can be seen from Figure 3.3C. In this figure the spatial distribution is stratified into five categories delimited by the 0, 20, 40, 60, and 80 percentiles to minimize the large discrepancies of large, populated areas. As with the number of ignitions, the population density shows zonal and meridional contrasts, with a densely populated coastline north of the Tagus and along the Algarve coastline and the inland region south of the Tagus with very low population density values. Figure 3.3 shows that densely populated areas are more prone to higher number of ignitions. Nonetheless these locations present lower fuel availability (Figure 3.3D) and greater vigilance from the populations to prevent, combat and control the spreading of wildfires (Lasslop & Kloster, 2017; Marques et al., 2011).

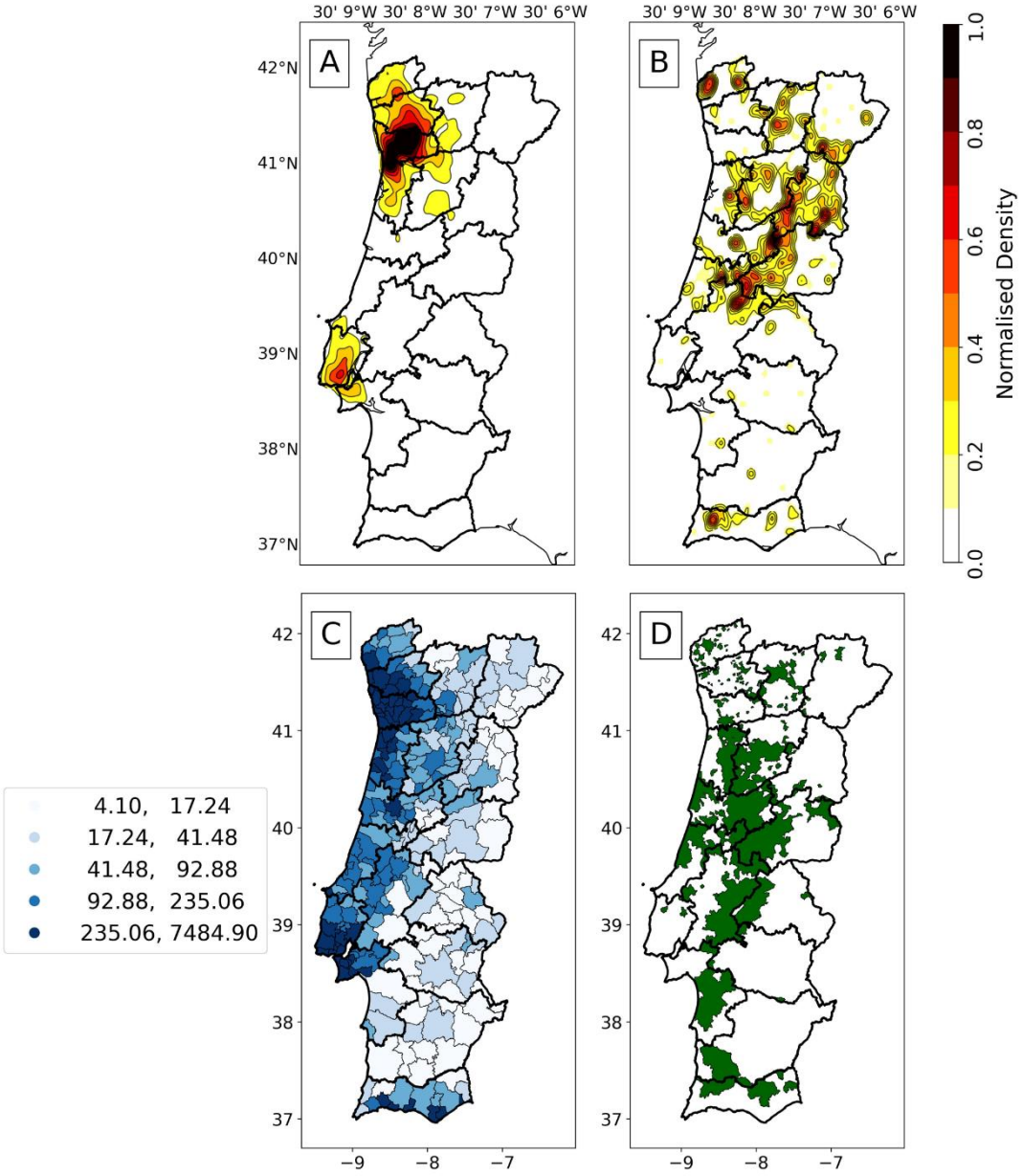

Figure 3.3 – Normalized Density geographical distribution for the A) number of ignitions and B) number of ignitions that exceeded the 1 000 ha of burned area. Annual mean value of population density per municipality is shown in C) stratified into 5 classes delimited by the 0, 20, 40, 60, 80 and 100 percentiles. Forest regions from COS2018 are presented in D).

On the other hand, the distribution of ignitions which exceeded 1 000 ha is more prevalent in the interior of the country (Figure 3.3B), Beira region, northern mountainous areas, as well as in the Algarve area, in the south. The Portuguese forested area is more prevalent in locations with lower population density (Figure 3.3C), which results from the fact that people have been abandoning the interior of the country to the largest cities on the coastal areas. Consequently, a larger area of land is left unmaintained, and thus with larger fuel availability for wildfire occurrence (Pereira et al., 2005). Furthermore, less population implicates lower vigilance in those areas and containing wildfires harder, hence larger burned areas from a single ignition, signaling more severe events (Pereira et al., 2011).

3.2 Fire Weather Index

The pixel-mean distribution for the extended summer (JJASO) for the 2001-2020 period of ISI, BUI and FWI, is shown in Figure 3.4. All indices present a sharp NW-SE gradient, with the values increasing towards the inland south of Alentejo, and with minimum values near Minho. These spatial distributions are explained by the climatological characteristics of Portugal. The gradient is mainly due to the prevalence of higher temperatures in the south when compared with the northern part of the country as well as to the amount of precipitation that is larger in the northern half of the territory (Cunha et al., 2011; Owens et al., 2021).

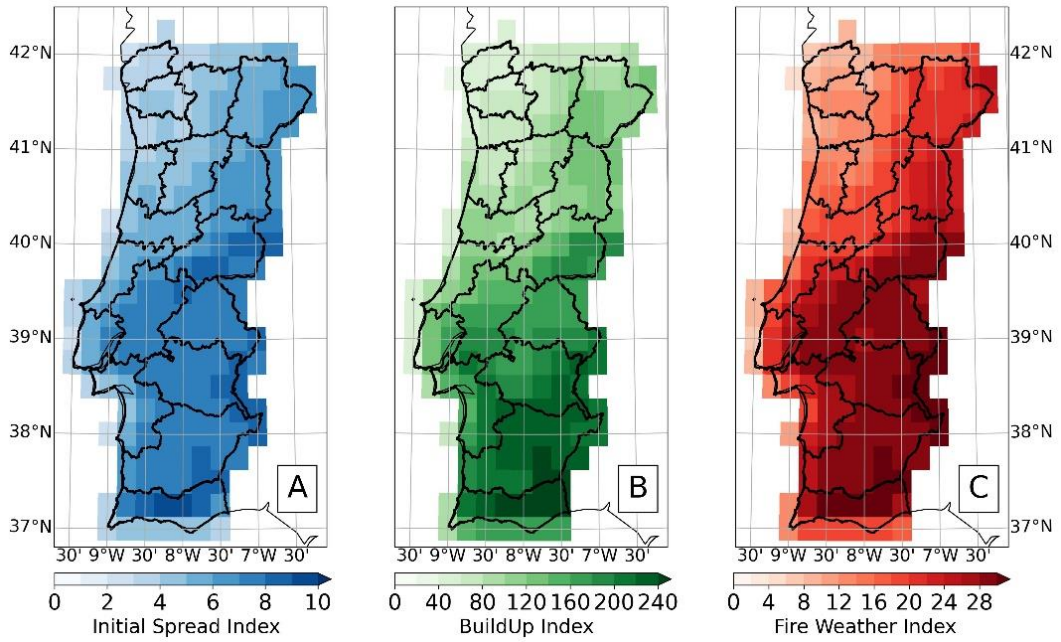

Figure 3.4 – Geographical distribution of mean values for the Extended Summer (JJASO) of A) Initial Spread Index, B) Buildup Index and C) Fire Weather Index.

For ISI (Figure 3.4A), which is calculated with the moisture content of surface litter and wind speed, its value increases where or when humidity is lower and wind speed is higher. Thus, in the southern areas the ISI is higher due to the typically dryer air during summer, usually advected from the African continent southeast (Cunha et al., 2011) which, combined with intense oceanic surface winds results in higher ISI values. Additionally, in the mountainous areas in central inland Portugal we can also observe moderate values associated with more intense winds due to the more complex topography. In the case of BUI (Figure 3.4B), a similar reasoning can be applied since the index depends on humidity content at deeper levels, and additionally on the temperature since it impacts the drying rate. The combined

effects of the gradient observed in both the rate at which a fire will spread when the fine fuel is dry (ISI) and the total fuel available to the spreading fire (BUI) explain in the gradient observed in the meteorological fire danger index (FWI) (Figure 3.4C).

The seasonal cycle of the three indices is shown in Figure 3.5. ISI (Figure 3.5A) presents a range of values varying between 0 and 12, with most of the maximum values being registered during the warmer months (JJA). Overall, ISI presents a large variability although the changes throughout the year are essentially marked by two peaks, a secondary one in March and the larger one centered in July, and the minimum values concentrating in the winter months. The transition seasons (spring and autumn) are those that present the widest range of values mainly due to occasional transient mid-latitude cyclones which typically transport a large amount of humidity and produce considerable precipitation and wind (Cunha et al., 2011; Owens et al., 2021). In the case of the BUI (Figure 3.5B), the nature of the seasonal distribution differs substantially. Presenting values between 0 and nearly 300, the variability of BUI is much lower in most humid months increasing gradually until autumn., BUI also presents a growth in the same period dramatically decreasing as the amount of precipitation climatologically increases (Cunha et al., 2011). Due to the nature of the two sub-indexes that determine BUI, the evolution is gradual until the warmest months (JJA), with both the temperature increase and humidity decrease gradually. When the first rains occur one of these sub-indexes is affected (DMC) on the short-term, while the other slowly decreases (DC) thus resulting in higher variability during this transition period depending on the occurrence of precipitation and, conversely, the temperature decreases in this period leading to an overall decrease of BUI (Van Wagner, 1987). When compared with ISI and BUI, FWI (Figure 3.5C) has a better-defined seasonality with higher values in the summer months, presenting the larger median values around 30 and 95th percentile maximums reaching 40. Similarly, the variability is greater in the transition months while the coldest and wettest months show values close to zero and lower variability.

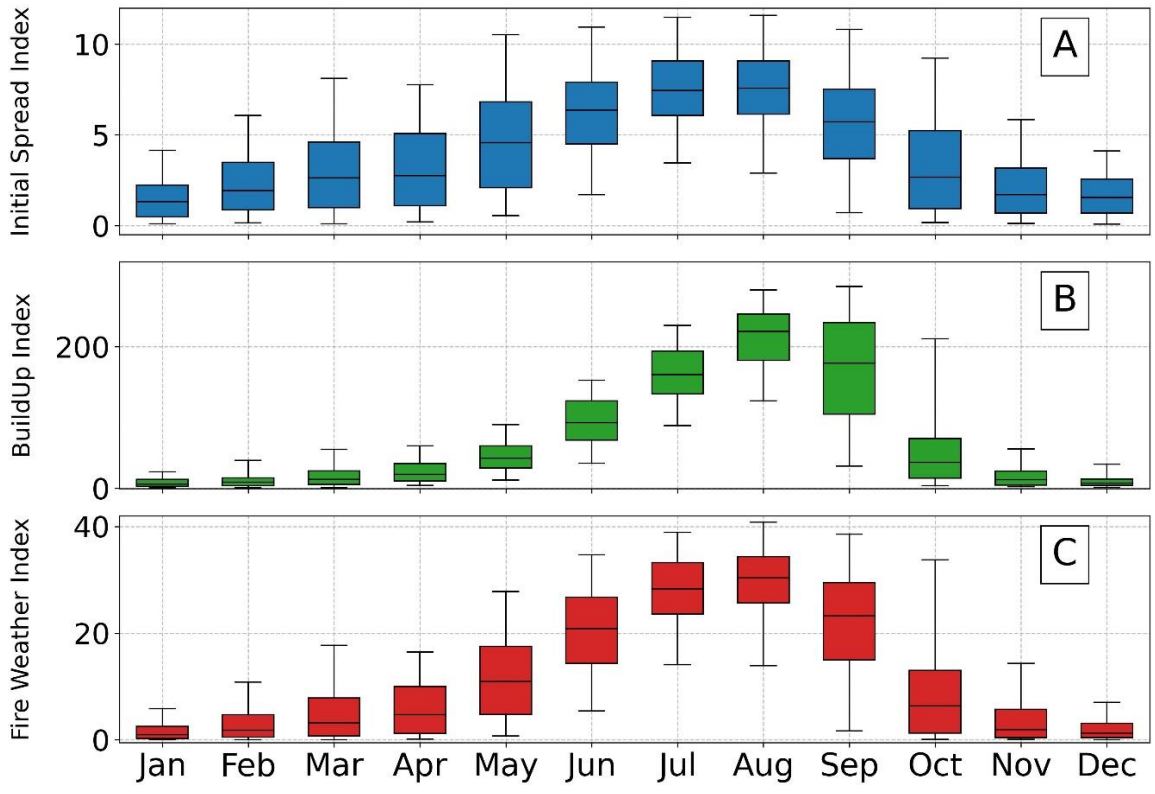

Figure 3.5 – Boxplot showing evolution of the yearly distribution for each index in the 2001-2020 period for A) Initial Spread Index, B) Buildup Index and C) Fire Weather Index.

Figure 3.6 shows a scatter plot of values of ISI versus BUI, with the observations stratified into two major groups, respectively those associated to ignitions originating burned area below (grey) and above (orange) 1 000 ha. The median values of BUI and ISI of each subgroup are represented by the two bold circles and the interquartile ranges of BUI and ISI are represented by the horizontal and the vertical lines. Ignitions associated to burned areas below 1 000 ha (grey dots) are associated to lower values of BUI, ISI, and therefore FWI (whose contour lines are represented by the labelled thin black curves). The median value of BUI of this group is about 100 and of ISI is around 6. The group of ignitions originating burned areas above 1 000 ha has much larger median values of BUI and ISI, respectively about 200 and 12. As to be expected observations belonging to this group tend to spread over regions associated to higher values of FWI. Furthermore, the evolution of the FWI in the last 40 years has been evaluated and crucial upward trends have been found in southwest and east Iberia in the last 3 decades; this work has been peer-reviewed and published (Santos et al., 2023) and can be found in the *supplemental material*.

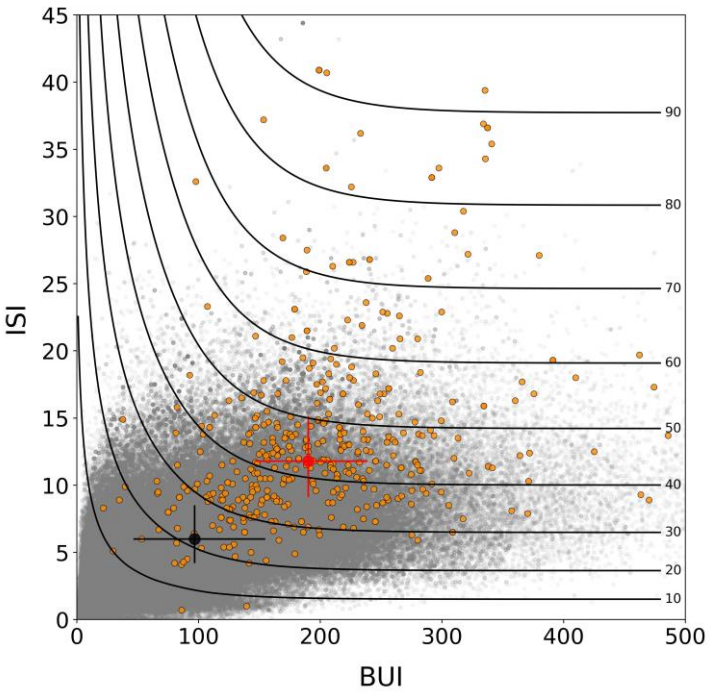

Figure 3.6 – FWI as a function of BUI and ISI. Values for the ignitions below 1 000 ha of burned area are represented by grey scatters with the black dot representing the median, the vertical and horizontal black lines delimit the 25th and 75th percentiles. Orange scatters represent ignitions that exceeded the 1 000 ha of burned area with median and percentiles represented the same way in red. The black curves correspond to different FWI isolines between 10 and 90.

3.3 Wind behavior

As mentioned, wind is an important agent in regulating both speed and direction of fire spread (Pinto et al., 2018b), as such, a climatological analysis of the wind field in continental Portugal essentially contributes to understanding any predisposition for an increase in wildfire potential during the fire season. The intra-annual distribution of the wind field for the study period over mainland Portugal is shown in Figure 3.7. For this purpose, hourly wind data was used to compute the mean daily value for each pixel, and then computing the spatial average over the territory. Finally, we distributed the days among eight sectors according to wind direction. An annual cycle is clearly defined throughout the months, with a prevalence of northwesterly (NW) winds (turquoise band) in the warmest months (May-September) that are steered by the Azores high pressure system that is located between the Azores and

the Madeira archipelagos during that time of the year (Trigo et al., 2000). In the cooler months (October - April) there is an increase of easterly (E), southeasterly (SE), and southerly (S) winds (purple, orange and red bands, respectively).

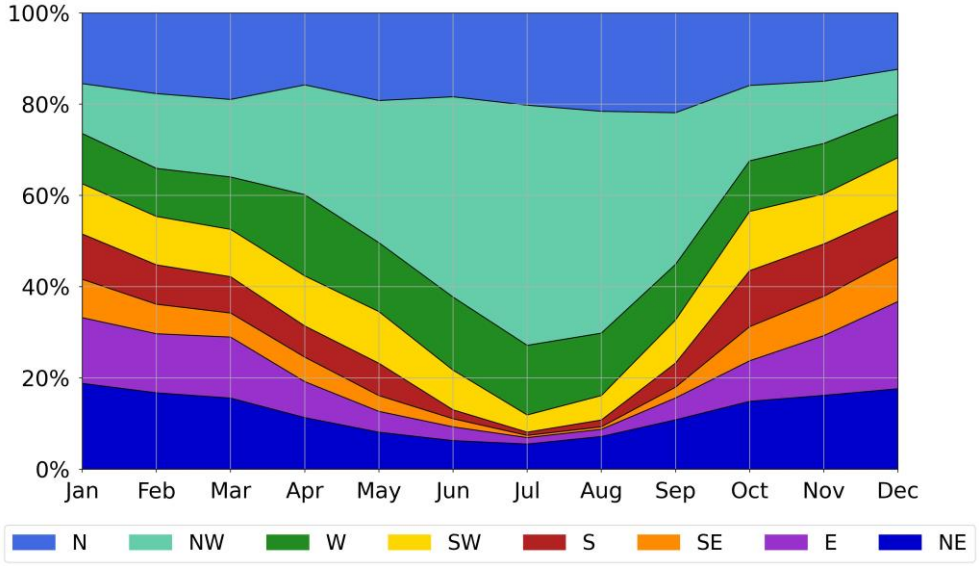

Figure 3.7 – Intra-annual fraction for each meteorological wind direction in Portugal for the 2001-2020 period.

The distribution of daily wind in Portugal at 12 UTC for the extended summer period (JJASO) of 2001-2020 is shown in Figure 3.8A, counting with a total of 596 700 vectors (195 pixels that cover the territory per 3 060 days). On the other hand, the distribution of the wind at 12UTC for the days with ignitions associated with burned area above 1 000 ha at ignition point is shown in Figure 3.8B, with a total of 421 vectors (421 ignition points). When considering all days and all pixels (Figure 3.8A), there is a prevalence of NW winds, followed by westerly (W) and southwesterly (SW) winds, but when the analysis restricts to the days with ignitions exceeding 1 000 ha of burned area at the ignition point (Figure 3.8B), there is a decrease in W winds accompanied by an increase in the E ones, with a substantial increment of the E and NE components representing 17.8% each. This change is well known for Portugal, as discussed in the *Introduction*, with the E wind component contributing with near 300 000 ha to the total 1 551 880 ha (for the 2001-2020 period), which represents near 20%, considering ignitions from Figure 3.8B.

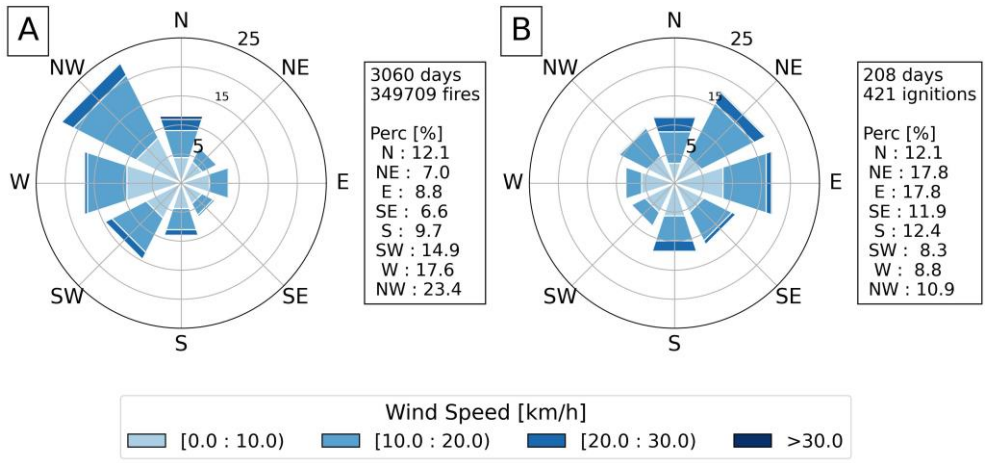

Figure 3.8 – Windrose for the Extended Summer (JJASO) for the 2001-2020 period considering A) all the 195 pixels for all days and B) days with ignitions that exceeded 1 000 ha of burned area at the ignition pixel.

3.4 Fires above 1 000 ha

Since a given burned area scar can be associated with different ignitions, FRP data was used together with available literature to discriminate the different fire episodes. The case of the Monchique wildfire events that took place in 2003 (Tedim et al., 2013) is shown in Figure 3.9. In August (Figure 3.9A), two distinct wildfire events took place in the area, which can be identified by the sets of FRP hotspots; in September (Figure 3.9B) FRP hotspots allow identifying a third event. This type of analysis was applied to other burn scars, and cases that were not reliably identified were not considered for analysis. Therefore, from the 426 ignitions with more than 1 000 ha of burned area, a total of 266 wildfires were considered (0.06% of all ignitions) which account for a total accumulated burned area of 1 381 582.6 ha (about 47.7% of the total). The discrepancy between the low fraction of wildfires (0.06%) and the high fraction of burned area (47.7%) indicates that a very small number of wildfires represents a substantial amount of burned area. Furthermore, as shown in Table 3.2, a substantial fraction is associated to scars with an elongated shape, strongly suggesting investigating the alignment between wind direction and landscape orientation.

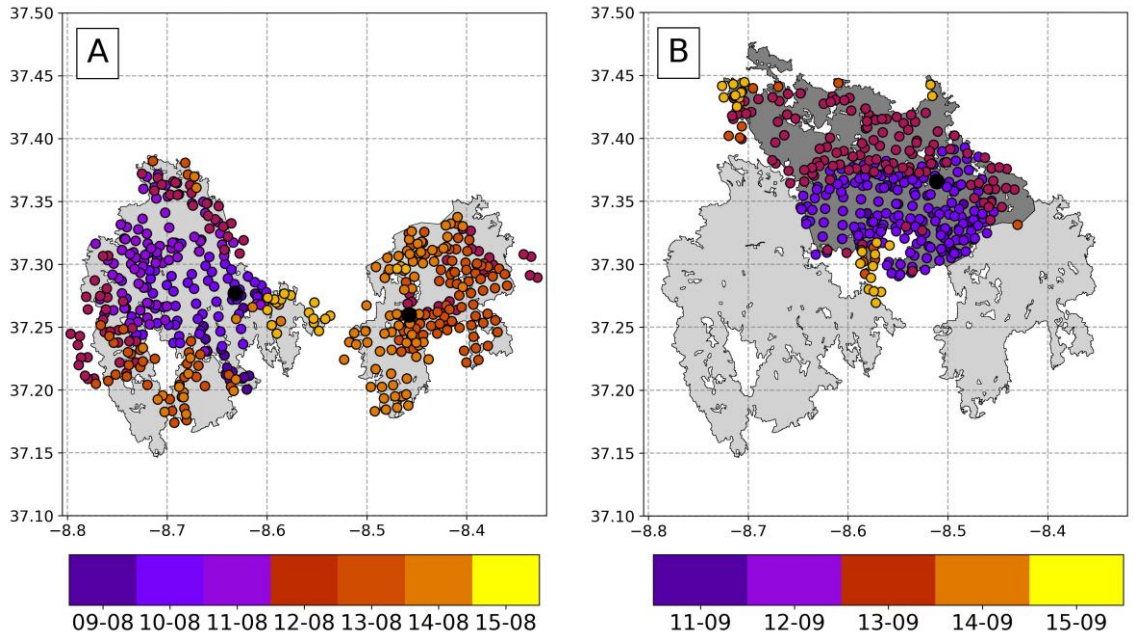

Figure 3.9 – Burned area shapes and hotspots (FRP's, colors corresponding to days) for the Monchique wildfires in 2003 during A) August and B) September. Dim grey represents the August burned area while the dark grey represents the September one, with the black dots marking the first ignition point. Adapted from Santos et. al 2023.

Table 3.2 – Same as Table 3.1 for the selected fires with more than 1 000 ha of burned area.

	Number of events	Burned area [ha]
Fires above 1000 ha	266 (0.06% of total)	1 381 582.6 (47.7%)
Elongated shape	208 (78.2% of 266)	1 068 140.6 (36.9%)
Wind prevalence	152 (73.1% of 208)	790 615.2 (27.3%)
Aligned	126 (82.9% of 152)	701 412.0 (24.2%)

3.4.1 Wildfires with an elongated shape

Elongated burned area shapes were identified by applying PCA to the spatial coordinates of pixels of each one of the selected 266 scars. The burned scar was classified as an *elongated shape* when the first PC accounted for more than 70 % of the spatial variance. As an example, Figure 3.10A presents the case for the scar from the Monchique wildfire event of 2018, which resulted 41 injuries, nearly 27 000 ha burned, as well as the loss of more than animals [2]. For this case, the first PC (black arrow) accounts for 76.4 % of the total variance (grey shape in Figure 3.10A).

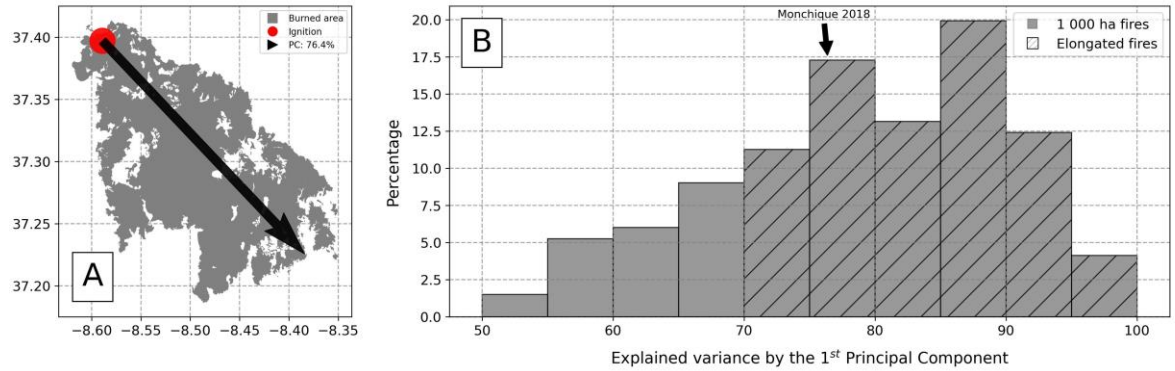

Figure 3.10 – A) Real world example of the PC methodology applied to the 2018 3rd of August Monchique wildfire. B) Distribution of the variability explained by the first PC of the 266 wildfires exceeding 1 000 ha. Black stripes delimit the selection of elongated fires with the black arrow indicating Monchique class (A).

Overall results for the 266 wildfire events are shown in Figure 3.10B. The figure depicts the distribution of explained variance by the first PC, with the minimum threshold of 70% being indicated by the striped bars, and the case of Monchique in 2018 (with 76.4% of variance explained) being marked by the black arrow. As a result of this analysis, 208 fire scars (78.2 % of 266, Table 3.2) were classified as *elongated shapes*, which correspond to more than a million ha (~37 %, Table 3.2) of burned area.

3.4.2 Wildfires with prevalence wind contribution

The role of wind was then investigated by filtering the fire events associated to especially intense winds. This was done by selecting cases where the mean of winds exceeding the 75th percentile of all winds observed during the episode was larger than 10 km/h (considered as a *Gentle Breeze* by the Beaufort Wind Scale, MetMatters, 2022). These cases correspond to situations where the most intense winds conserve direction over time, thus being dubbed as fire episodes with *prevalent wind contribution*.

Figure 3.11 shows the distribution of wind direction (light blue arrows), with the winds above the 75th percentile (red arrows, wind speed above 20.6 km/h) and their mean (dark blue arrow, with a wind speed average of 23.4 km/h) for the case of the Monchique fire event of August 2018 (Figure 3.10A).

Looking at the 75th percentile of the wind speed during the 266 fire episodes the majority of them (circa 80 %) surpassed 10 km/h. This reveals that these fires are associated with very intense winds, a condition that is favorable to fire propagation and consequently large, burned areas. The cases with means above the threshold will present a substantial effect on the prevalent circulation near the ground

[2] https://24.sapo.pt/atualidade/artigos/contacto-de-cabo-eletrico-com-eucalipto-causou-fogo-de-monchique-em-2018

and, expectedly, on wildfire propagation. As a result of this analysis, 152 fire scars (73.1% of 208, Table 3.2) were classified as *prevalent wind contribution*, which correspond to nearly 800 000 ha (~27 %, Table 3.2).

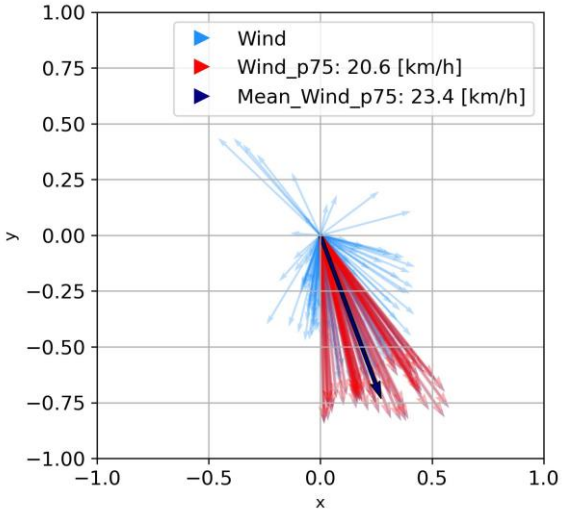

Figure 3.11 – Wind field for the same example as in Figure 3.10. Light blue vectors represent the hourly wind and the dark blue vector the mean of the winds above the 75th percentile of wind speed.

3.4.3 Aligned wildfires

We finally defined *aligned fires* as those where the angle between the mean wind computed over observed winds above the 75th percentile and the burned area first PC is lower than 45º. Figure 3.12A presents the case of the Monchique fire event of August 2018, (Figure 3.10A and Figure 3.11) where the angle is 23º.

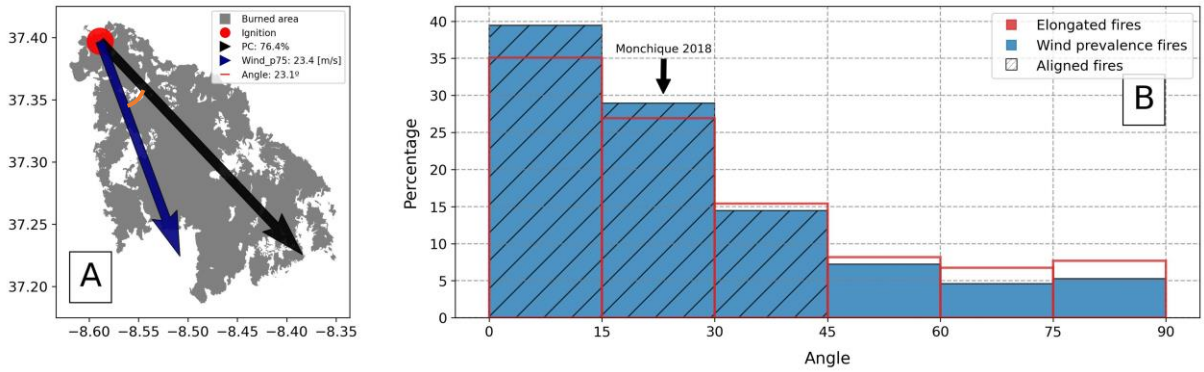

Figure 3.12 – A) Representation of the burned shape PC (black vector), mean of the winds above the 75th percentile of wind speed (dark blue vector) and the angle between them (orange line) for the same example from Figure 3.11. B) Distribution of the angle made by the vectors described in (A) for the 208 elongated fires (red) and the 156 wind prevalence fires (blue). Black stripes delimit the top for the selection of wind prevalence fires with the black arrow indicating Monchique class (A).

Two histograms for the angles are shown in Figure 3.12B, respectively for *elongated fires* (red), and for fires with *prevalent wind contribution fires* (blue), with the maximum threshold of 45º indicated by the black stripes and the case of Monchique 2018 (with an angle of 23.1º) marked by the black arrow. Shared between the two distributions, is the fact that there is a greater density in lower angles, with angles above 45º being clearly the minority. It may be noted that fires with wind fire prevalence present

slightly higher (lower) frequencies for the lower (higher) angles. As a result of this analysis, 126 fires (82.9 % of the 152, Table 3.2) were classified as *aligned*, which correspond to nearly 700 000 ha (~24 %, Table 3.2).

The distribution of the 126 *aligned wildfires*, presented in Figure 3.13, is similar to the geographical distribution seen in Figure 3.3B, with a prevalence of occurrence inside the forested areas (Figure 3.3D), mainly in center Portugal where the topography is more complex.

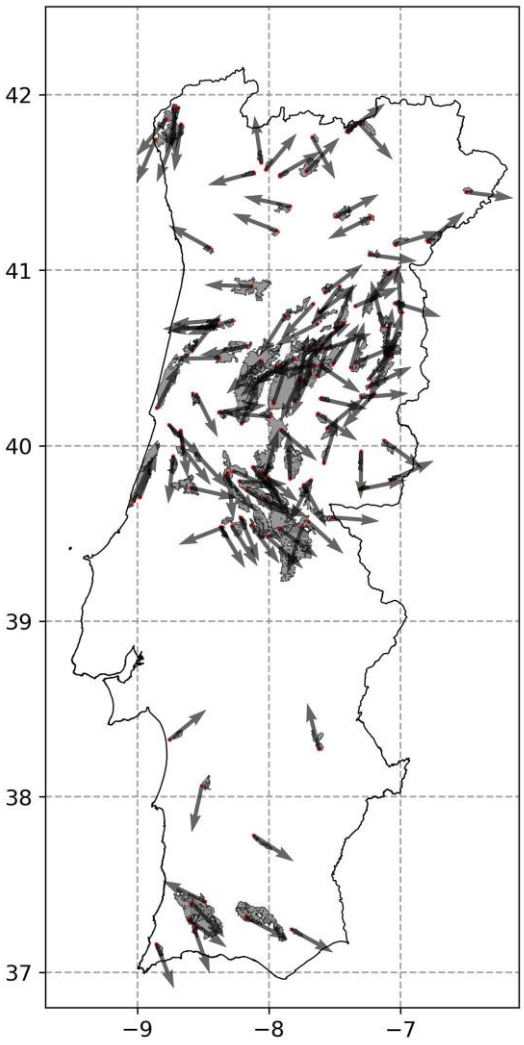

Figure 3.13 – Representation of the 126 aligned fires scars with associated PC.

Chapter 4 Conclusions

This main aim of the thesis was to assess the role played by the wind in large fire events in continental Portugal. Wildfires, namely the most catastrophic ones, are landmark events in Portugal, and in the last decades, several of these large events had strong impacts on society. This work relied on FWI to rate meteorological fire danger and characterized its climatology and evolution in Portugal. The wind field associated to the largest wildfires in the last two decades was analyzed in order to assess the role played by wind in triggering these events.

As expected from previous studies, no relation was found between the number of ignitions and burned area, a feature that is explained since higher burned areas depend on factors such as favorable weather conditions, available fuel to burn, besides an ignition to generate fire. Three major episodes were identified in 2003, 2005, and 2017, the first and last with the largest burned area and the middle one with the largest number of ignitions. The monthly variability presented two peaks, a major one and a secondary one, the first smaller peak in the month of March, related to human inflicted controlled burnings, and the following larger one in July, August, and September, corresponding to the summer-period. The analysis of these values was further carried out by analyzing spatial KDE plots, which revealed that the number of ignitions was mostly concentrated near the greatest population centers of Porto, lower Minho, and Lisbon. On the other hand, the larger burned area is observed in an overlapping area of lower population density and highly forested regions in the Beira and Algarve regions. This discrepancy between the areas of ignitions and burned area is easily explained by the fact that high density areas do have more vigilance while the less populated do not, besides, these areas also have greater unmaintained land thus leading to more fuel availability for wildfire progression. In this regard, in the 2001-2000 period, about 0.10 % of ignitions (426) exceeded 1 000 ha burned area and 60 % of these (266, 0.06 % of the total) accounted for nearly 50 % of all burned area.

The geographical distribution of FWI showed a NW-SE gradient with its values increasing towards the south. This distribution relates to the climatology of the country, with the northern part being more humid while the south is arid with higher temperatures. Two sub-indexes (ISI and BUI) were also analyzed and presented a similar geographical arrangement. These three variables were observed to have higher values in the summer, in the months of JJA. Both the ISI and BUI present different evolutions depending on their inherent characteristics, with the former evolving smoothly throughout the year while the latter grows until the end of the summer where it presents a more abrupt decrease at the beginning of autumn, mainly due to an increment of humidity at this time of year. Consequently, the FWI follows these distributions, with summer median values around 25 and extreme values topping at around 40. Furthermore, the relation of these three variables was analyzed per ignition observation, with the group of ignitions exceeding 1000 ha markedly representing the conditions of higher fire danger, with greater index values.

The analysis of the wind field in continental Portugal showed that there is a well-defined annual cycle. In the winter months the circulation is predominantly from east, southeast, and south, while the warmest months, between May and September, presents a strong northwesterly component. In days that exceeded 1 000 ha burned, pixels which saw ignitions between 2001 and 2020 in the extended summer period showed a prevalence of easterly winds, differing substantially to the prevalent circulation in this period of the season. A sample of 266 wildfires associated to a burned area larger than 1 000 ha and representing nearly 50 % of burned area in 2001-2020 was selected and, using PCA, 208 events were classified as long shape wildfires (those where the first principal component explained more than 70 % of the total spatial variance of the scar). A filter was then used that retained 152 events where the length

of the vectorial mean of the winds with intensity above the 75th percentile was larger than 10 km/h. Finally, a subset of aligned fires was obtained by restricting to fires where the direction of the first PC with the mean wind was below 45º. The set of aligned fires represent 24.2 % of all burned area in the 2001-2020 period. These wildfires were mostly observed in the center of the territory where the topography is more complex, and the wind field associated with them presented a larger NW and S component, coinciding with the orientation of the forested areas.

This work stresses the importance of the role played by wind in large fire events in Portugal and points out that wildfires are not directly linked to a single type of wind direction, but also to the geographical location where they occur. Thus, considering that a small part of filtered ignitions (0.03 % from total) is responsible for a substantial part of burned area (24.2 % from total), when wind direction is appropriate (and if all other conditions are met, such as fuel presence), then a small ignition can grow into a large uncontrolled wildfire. It is, therefore, appropriate to consider the wind direction when analyzing fire danger indexes such as the FWI and this parameter is certainly an added value to fire prevention and management.

References

Abatzoglou, J. T., Williams, A. P., & Barbero, R. (2019). Global emergence of anthropogenic climate change in fire weather indices. Geophysical Research Letters, 46(1), 326-336. https://doi.org/10.1029/2018GL080959

Alcubierre, P. C., Ribau, M. C., de Egileor, A. L. O., Bover, M. M., & Kraus, P. D. (2011). Prevention of large wildfires using the fire types concept. Barcelona, Spain: Generalitat de Catalunya.

Alexander, M.E. 1994. Proposed revision of fire danger class criteria for forest and rural areas in New Zealand. National Rural Fire Authority, Wellington, in association with the New Zealand Forest Research Institute, Rotorua. 62p.

Amatulli, G., Camia, A., & San-Miguel-Ayanz, J. (2013). Estimating future burned areas under changing climate in the EU-Mediterranean countries. Science of the total environment, 450, 209-222. https://doi.org/10.1016/j.scitotenv.2013.02.014

Amraoui, M., Pereira, M. G., DaCamara, C. C., & Calado, T. J. (2015). Atmospheric conditions associated with extreme fire activity in the Western Mediterranean region. Science of the total environment, 524, 32-39. https://doi.org/10.1016/j.scitotenv.2015.04.032

Artés, T., Oom, D., De Rigo, D., Durrant, T. H., Maianti, P., Libertà, G., & San-Miguel-Ayanz, J. (2019). A global wildfire dataset for the analysis of fire regimes and fire behaviour. Scientific data, 6(1), 296. https://doi.org/10.1038/s41597-019-0312-2

Barros, A. M., Pereira, J. M., & Lund, U. J. (2011). Identifying geographical patterns of wildfire orientation: A watershed-based analysis. Forest ecology and management, 264, 98-107. https://doi.org/10.1016/j.foreco.2011.09.027

Bickerton, J. (2012). The fire triangle. Loss Prevention Bulletin, (226).

Carmo, M., Ferreira, J., Mendes, M., Silva, Á., Silva, P., Alves, D., ... & Xavier Viegas, D. (2021). The climatology of extreme wildfires in Portugal, 1980–2018: Contributions to forecasting and preparedness. International Journal of Climatology. https://doi.org/10.1002/joc.7411

Cresswell-Clay, N., Ummenhofer, C. C., Thatcher, D. L., Wanamaker, A. D., Denniston, R. F., Asmerom, Y., & Polyak, V. J. (2022). Twentieth-century Azores High expansion unprecedented in the past 1,200 years. Nature Geoscience, 15(7), 548-553. https://doi.org/10.1038/s41561-022-00971-w

Cunha, S., Silva, Á., Herráez, C., Pires, V., Chazarra, A., Mestre, A., Nunes, L., Mendes, M., Neto, J., Marques, J., Mendes, L. (2011). Atlas Climático Ibérico – Iberian Climate Atlas

DaCamara, C. C., Calado, T. J., Ermida, S. L., Trigo, I. F., Amraoui, M., & Turkman, K. F. (2014). Calibration of the fire weather index over mediterranean europe based on fire activity retrieved from msg satellite imagery. International Journal of Wildland Fire, 23(7), 945–958. https://doi.org/10.1071/WF13157

de Groot, W. J. D., Field, R. D., Brady, M. A., Roswintiarti, O., & Mohamad, M. (2007). Development of the Indonesian and Malaysian fire danger rating systems. Mitigation and Adaptation Strategies for Global Change, 12, 165-180. https://doi.org/10.1007/s11027-006-9043-8

Di Castri, F. (1991). An ecological overview of the five regions of the world with Mediterranean climate. Biogeography of Mediterranean invasions, 3-15.

Direção-Geral do Território, 2019. Especificações técnicas da Carta de Uso e Ocupação do Solo (COS) de Portugal Continental para 2018. Relatório Técnico. Direção-Geral do Território. [http://mapas.dgterritorio.pt/atom-dgt/pdf-cous/COS2018/ET-COS-2018_v1.pdf]

Dowdy, A. J., Mills, G. A., Finkele, K., & De Groot, W. (2009). Australian fire weather as represented by the McArthur forest fire danger index and the Canadian forest fire weather index (p. 91). Melbourne: Centre for Australian Weather and Climate Research.

Ermitão, T., Gouveia, C. M., Bastos, A., & Russo, A. C. (2022). Interactions between hot and dry fuel conditions and vegetation dynamics in the 2017 fire season in Portugal. Environmental Research Letters, 17(9), 095009. https://doi.org/10.1088/1748-9326/ac8be4

European Centre for Medium-Range Weather Forecasts (ECMWF). "ERA5: How to calculate wind speed and wind direction from u and v components of the wind?". Consulted in February 2022, https://confluence.ecmwf.int/pages/viewpage.action?pageId=133262398

Fernandes, P. M., Monteiro-Henriques, T., Guiomar, N., Loureiro, C., & Barros, A. M. (2016). Bottom-up variables govern large-fire size in Portugal. Ecosystems, 19(8), 1362-1375. https://doi.org/10.1007/s10021-016-0010-2

Fotheringham, A. S., Brunsdon, C., and Charlton, M. (2000). Quantitative Geography: Perspectives on Spatial Data Analysis. London, United Kingdom: Sage.

Freire, J. G., & DaCamara, C. C. (2019). Using cellular automata to simulate wildfire propagation and to assist in fire management. Natural hazards and earth system sciences, 19(1), 169-179. https://doi.org/10.5194/nhess-19-169-2019

García-Herrera, R., Garrido-Perez, J. M., Barriopedro, D., Ordóñez, C., VicenteSerrano, S. M., Nieto, R., et al. (2019). The European 2016/17 Drought. J. Clim. 32 (11), 3169–3187. https://doi.org/10.1175/JCLI-D-18-0331.1

Giglio, L., Schroeder, W., Hall, J. V., & Justice, C. O. (2018). MODIS Collection 6 Active Fire Product User's Guide Revision B. Department of Geographical Sciences. University of Maryland, 9. https://doi.org/10.1016%2Fj.rse.2016.02.054

Gómez-González, S., Ojeda, F., & Fernandes, P. M. (2018). Portugal and Chile: Longing for sustainable forestry while rising from the ashes. Environmental Science & Policy, 81, 104-107. https://doi.org/10.1016/j.envsci.2017.11.006

Hersbach, H., Bell, B., Berrisford, P., Hirahara, S., Horányi, A., Muñoz-Sabater, J., Nicolas, J., Peubey, C., Radu, R., Schepers, D., et al. (2020). The era5 global reanalysis. Quarterly Journal of the Royal Meteorological Society, 146(730), 1999–2049. https://doi.org/10.1002/qj.3803

Jolliffe, I. T. (2002). Principal component analysis for special types of data (pp. 338-372). Springer New York. https://doi.org/10.1007/0-387-22440-8_13

Kautz, L. A., Martius, O., Pfahl, S., Pinto, J. G., Ramos, A. M., Sousa, P. M., & Woollings, T. (2022). Atmospheric blocking and weather extremes over the Euro-Atlantic sector–a review. Weather and Climate Dynamics, 3(1), 305-336. https://doi.org/10.5194/wcd-3-305-2022

Lasslop, G., & Kloster, S. (2017). Human impact on wildfires varies between regions and with vegetation productivity. Environmental Research Letters, 12(11), 115011. https://doi.org/10.1088/1748-9326/aa8c82

Lawrence, M. G. (2005). The relationship between relative humidity and the dewpoint temperature in moist air: A simple conversion and applications. Bulletin of the American Meteorological Society, 86(2), 225–234. https://doi.org/10.1175/BAMS-86-2-225

Lecina-Diaz, J., Alvarez, A., & Retana, J. (2014). Extreme fire severity patterns in topographic, convective and wind-driven historical wildfires of Mediterranean pine forests. PloS one, 9(1), e85127. https://doi.org/10.1371/journal.pone.0085127

Lehtonen, I., Ruosteenoja, K., Venäläinen, A., & Gregow, H. (2014). The projected 21st century forest-fire risk in Finland under different greenhouse gas scenarios.

Leone, V., Lovreglio, R., Martín, M. P., Martínez, J., & Vilar, L. (2009). Human factors of fire occurrence in the Mediterranean. In Earth observation of wildland fires in Mediterranean ecosystems (pp. 149-170). Springer, Berlin, Heidelberg. https://doi.org/10.1007/978-3-642-01754-4_11

Lionello, P., Malanotte-Rizzoli, P., Boscolo, R., Alpert, P., Artale, V., Li, L., ... & Xoplaki, E. (2006). The Mediterranean climate: an overview of the main characteristics and issues. Developments in earth and environmental sciences, 4, 1-26. https://doi.org/10.1016/S1571-9197(06)80003-0

Marques, S., Borges, J.G., Garcia-Gonzalo, J., Moreira, F., Carreiras, J. M. B., Oliveira, M. M., Cantarinha, A., Botenquim, B., & Pereira, J. M. C. (2011). Characterization of wildfires in Portugal. Eur J Forest Res 130, 775–784. https://doi.org/10.1007/s10342-010-0470-4

Martins, V., Miranda, A. I., Carvalho, A., Schaap, M., Borrego, C., & Sá, E. (2012). Impact of forest fires on particulate matter and ozone levels during the 2003, 2004 and 2005 fire seasons in Portugal. Science of the Total Environment, 414, 53-62. https://doi.org/10.1016/j.scitotenv.2011.10.007

MetMatters, Royal Meteorological Society. "The Beaufort Wind Scale". Consulted in February 2022, https://www.rmets.org/metmatters/beaufort-wind-scale

Moritz, M. A., Morais, M. E., Summerell, L. A., Carlson, J. M., & Doyle, J. (2005). Wildfires, complexity, and highly optimized tolerance. Proceedings of the National Academy of Sciences, 102(50), 17912-17917. https://doi.org/10.1073/pnas.0508985102

Mota B, Freire JG, Oliveira M, Nunes SA, Dilão R, DaCamara CC (2022)," Using cellular automata to assess the role played by wind direction in two large fire episodes in Portugal". In "Advances in Forest Fire Research 2022" (Eds Domingos Xavier Viegas and Luís Mário Viegas). pp. 431-435. (Imprensa da Universidade de Coimbra, eISBN 978-989-26-2298-9) https://doi.org/10.14195/978-989-26-2298-9_69

Nunes, S. A., DaCamara, C. C., Turkman, K. F., Calado, T. J., Trigo, R. M., & Turkman, M. A. (2019). Wildland fire potential outlooks for Portugal using meteorological indices of fire danger. Natural Hazards and Earth System Sciences, 19(7), 1459-1470. https://doi.org/10.5194/nhess-19-1459-2019

Owen, L. E., Catto, J. L., Stephenson, D. B., & Dunstone, N. J. (2021). Compound precipitation and wind extremes over Europe and their relationship to extratropical cyclones. Weather and Climate Extremes, 33, 100342. https://doi.org/10.1016/j.wace.2021.100342

Pausas, J. G., & Keeley, J. E. (2019). Wildfires as an ecosystem service. Frontiers in Ecology and the Environment, 17(5), 289-295. https://doi.org/10.1002/fee.2044

Pereira, M. G., Calado, T. J., DaCamara, C. C., & Calheiros, T. (2013). Effects of regional climate change on rural fires in Portugal. Climate research, 57(3), 187-200. https://doi.org/10.3354/cr01176

Pereira, M. G., Malamud, B. D., Trigo, R. M., & Alves, P. I. (2011). The history and characteristics of the 1980–2005 Portuguese rural fire database. Natural Hazards and Earth System Sciences, 11(12), 3343-3358. https://doi.org/10.5194/nhess-11-3343-2011

Pereira, M. G., Trigo, R. M., da Camara, C. C., Pereira, J. M., & Leite, S. M. (2005). Synoptic patterns associated with large summer forest fires in Portugal. Agricultural and Forest Meteorology, 129(1-2), 11-25. https://doi.org/10.1016/j.agrformet.2004.12.007

Pinto, M. M., DaCamara, C. C., Hurduc, A., Trigo, R. M., & Trigo, I. F. (2020). Enhancing the fire weather index with atmospheric instability information. Environmental Research Letters, 15(9), 0940b7. https://doi.org/10.1088/1748-9326/ab9e22

Pinto, M. M., DaCamara, C. C., Trigo, I. F., Trigo, R. M., & Turkman, K. F. (2018a). Fire danger rating over mediterranean europe based on fire radiative power derived from meteosat. Natural Hazards and Earth System Sciences, 18(2), 515–529. https://doi.org/10.5194/nhess-18-515-2018

Pinto, M. M., Hurduc, A., Trigo, R. M., Trigo, I. F., & DaCamara, C. C. (2018b). The extreme weather conditions behind the destructive fires of June and October 2017 in Portugal. https://doi.org/10.14195/978-989-26-16-506_13

Ribeiro, L. M., Viegas, D. X., Almeida, M., McGee, T. K., Pereira, M. G., Parente, J., ... & Hardin, H. (2020). Extreme wildfires and disasters around the world: Lessons to be learned. In Extreme wildfire events and disasters (pp. 31-51). Elsevier. https://doi.org/10.1016/B978-0-12-815721-3.00002-3

Rodrigo, F. S. (2021). Exploring combined influences of seasonal East Atlantic (EA) and North Atlantic Oscillation (NAO) on the temperature-precipitation relationship in the Iberian Peninsula. Geosciences, 11(5), 211. https://doi.org/10.3390/geosciences11050211

San-Miguel-Ayanz, J., Durrant, T., Boca, R., Maianti, P., Libertá, G., Artés-Vivancos, T., … & Löffler, P. (2021). Forest Fires in Europe, Middle East and North Africa 2020 EUR 30862 EN, Publications Office of the european Union, Luxembourg. https://doi.org/10.2760/34094

Santos, L. C., Lima, M. M., Bento, V. A., Nunes, S. A., DaCamara, C. C., Russo, A., ... & Trigo, R. M. (2023). An Evaluation of the Atmospheric Instability Effect on Wildfire Danger Using ERA5 over the Iberian Peninsula. Fire, 6(3), 120. https://doi.org/10.3390/fire6030120

Santos, J., & Corte-Real, J. (2006). Temperature extremes in Europe and wintertime large-scale atmospheric circulation: HadCM3 future scenarios. Climate Research, 31(1), 3-18. https://doi.org/10.3354/cr031003

Schmuck, G., San-Miguel-Ayanz, J., Barbosa, P., Camia, A., Kucera, J., Liberta, G. (2004). Forest Fires in Europe – 2003 fire campaign S.P.I.04.124 EN, European Communities, Italy.

Schmuck, G., San-Miguel-Ayanz, J., Barbosa, P., Camia, A., Kucera, J., Liberta, G. (2006). Forest Fires in Europe 2005 EUR 22312 EN, European Communities, Italy.

Sousa, P. M., Trigo, R. M., Barriopedro, D., Soares, P. M., & Santos, J. A. (2018). European temperature responses to blocking and ridge regional patterns. Climate Dynamics, 50, 457-477. https://doi.org/10.1007/s00382-017-3620-2

Stocks, B. J., Cahoon, D. R., Levine, J. S., Cofer III, W. R., & Lynham, T. J. (1996). Major 1992 forest fires in central and eastern Siberia: satellite and fire danger measurements. In Fire in Ecosystems of Boreal Eurasia (pp. 139-150). Dordrecht: Springer Netherlands.

Syphard, A. D., & Keeley, J. E. (2015). Location, timing and extent of wildfire vary by cause of ignition. International Journal of Wildland Fire, 24(1), 37-47. https://doi.org/10.1071/WF14024

Tedim, F., Remelgado, R., Borges, C., Carvalho, S., & Martins, J. (2013). Exploring the occurrence of mega-fires in Portugal. Forest Ecology and Management, 294, 86-96. https://doi.org/10.1016/j.foreco.2012.07.031

Tipping, M. E., & Bishop, C. M. (1999). Mixtures of probabilistic principal component analyzers. Neural computation, 11(2), 443-482. https://doi.org/10.1162/089976699300016728

Trigo, R. M., & DaCamara, C. C. (2000). Circulation weather types and their influence on the precipitation regime in Portugal. *International Journal of Climatology: A Journal of the Royal Meteorological Society*, *20*(13), 1559-1581. https://doi.org/10.1002/1097-0088(20001115)20:13<1559::AID-JOC555>3.0.CO;2-5

Trigo, R. M., Pereira, J. M., Pereira, M. G., Mota, B., Calado, T. J., Dacamara, C. C., & Santo, F. E. (2006a). Atmospheric conditions associated with the exceptional fire season of 2003 in Portugal. International Journal of Climatology: A Journal of the Royal Meteorological Society, 26(13), 1741-1757. https://doi.org/10.1002/joc.1333

Trigo, R., Xoplaki, E., Zorita, E., Luterbacher, J., Krichak, S. O., Alpert, P., ... & Mariotti, A. (2006b). Relations between variability in the Mediterranean region and mid-latitude variability. In Developments in Earth and Environmental Sciences (Vol. 4, pp. 179-226). Elsevier. https://doi.org/10.1016/S1571-9197(06)80006-6

van Wagner, C. (1987). Development and structure of the canadian forest fireweather index system. Can. For. Serv., Forestry Tech. Rep.

Wang, Y., Anderson, K. R., Suddaby, R. M., et al. (2015). Updated source code for calculating fire danger indices in the canadian forest fire weather index system.

Supplemental material

A. An Evaluation of the Atmospheric Instability Effect on Wildfire Danger Using ERA5 over the Iberian Peninsula

Luana C. Santos, Miguel M. Lima, Virgílio A. Bento, Sílvia A. Nunes, Carlos C. DaCamara, Ana Russo, Pedro M. M. Soares, Ricardo M. Trigo

Paper published in *Fire* (Santos et al., 2023), https://doi.org/10.3390/fire6030120

fire

MDPI

Article

An Evaluation of the Atmospheric Instability Effect on Wildfire Danger Using ERA5 over the Iberian Peninsula

Luana C. Santos [1], Miguel M. Lima [1], Virgílio A. Bento [1], Sílvia A. Nunes [1], Carlos C. DaCamara [1], Ana Russo [1], Pedro M. M. Soares [1] and Ricardo M. Trigo [1,2,*]

[1] Faculdade de Ciências, Instituto Dom Luiz (IDL), Universidade de Lisboa, 1749-016 Lisboa, Portugal
[2] Departamento de Meteorologia, Universidade Federal do Rio de Janeiro, Rio de Janeiro 21941-919, Brazil
* Correspondence: rmtrigo@ciencias.ulisboa.pt

Abstract: The Fire Weather Index (FWI) is used to assess meteorological fire danger worldwide. It has been argued that it lacks an atmospheric instability term. A new enhanced FWI (FWIe) was recently developed incorporating atmospheric instability in the form of the Continuous Haines Index (CHI). Here, the first climatological and evolution analysis of these indexes was performed using ERA5 data for the 1980–2020 period. There was a prevalence of higher values over central Iberia; these were heavily modulated by the climate types, topography, and land cover. Southwest and east Iberia suffered the greatest decadal increases in all three indexes. Relating both indexes to occurrences detected by satellite, through fire radiative power (FRP), showed that FWIe provided an improved meteorological fire danger assessment in higher-risk conditions. This showed that greater-risk observations were more prone to be affected by atmospheric instability than lower-danger observations. Case studies for the 2017 central Portugal and 2003 and 2018 Monchique wildfires were additionally conducted to verify these conclusions. This work points to the usefulness of FWIe when/where atmospheric instability may play a critical role in the development of wildfires, which may contribute to a more focused deployment of suppression mechanisms by the authorities.

Keywords: Fire Weather Index; Continuous Haines Index; wildfires; Iberian Peninsula; fire radiative power; ERA5

Citation: Santos, L.C.; Lima, M.M.; Bento, V.A.; Nunes, S.A.; DaCamara, C.C.; Russo, A.; Soares, P.M.M.; Trigo, R.M. An Evaluation of the Atmospheric Instability Effect on Wildfire Danger Using ERA5 over the Iberian Peninsula. *Fire* **2023**, *6*, 120. https://doi.org/10.3390/fire6030120

Academic Editor: Grant Williamson

Received: 1 February 2023
Revised: 1 February 2023
Accepted: 11 March 2023
Published: 14 March 2023

1. Introduction

Wildfires are important extreme events that affect world ecosystems and human populations [1–3]. Wildfire behavior, namely the rate of spread and burning patterns, depends on a variety of factors, including ignition, topography, land cover, fire management and suppression policies, and weather conditions [1,4–6].

In the past few decades, several studies have analyzed the evolution of fire regimes over different regions of the world, taking into consideration ongoing global climate change [1,7–10]. In this regard, the Mediterranean basin has attracted special attention since it is recurrently subject to large wildfires, due to its warm and dry summers together with persistent heat spells [5,6,11,12]. Within the Mediterranean, the Iberian Peninsula (IP) is the area most affected by wildfires, representing more than 60% (about 11 million ha) of the total burned area of the five southern European Union (EU) Member States (i.e., Portugal, Spain, France, Italy, and Greece) [10,13]. This is even more relevant since Portugal and northwestern Spain (Galicia) is one of the most wildfire-prone areas in Europe [10], and future climate projections point to a substantial increase in fire danger for the next few decades [1,7–10]. Human-related factors also contribute to the existence of wildfires, with the Mediterranean regions showing the largest proportion of human-caused fires in the world, including the intentional or negligent use of fire or even inappropriate forestry management [14,15].

The highly favorable climate conditions observed in the IP are linked to the three main types of wildfires which often occur in the region, namely wind-driven, topo-graphic, and

plume-dominated or convective fires [16–18]. Wind-driven wildfires strongly depend on wind intensity and direction, with small changes in landscape and topography having virtually no impact on fire propagation [19]. Topographic fires are highly dependent on local-scale winds caused by differential solar heating (i.e., slope or valley winds and sea breezes), showing a strong day–night intensity change [20]. Plume-dominated (convective) fires are characterized by the presence of intense atmospheric instability allied with the accumulation and availability of fuels for fire development, normally being more intense (energetic) and with unpredictable behavior [21].

Several methods have been proposed to assess meteorological fire danger in different regions using the Canadian Forest Fire Weather Index System (CFFWIS) [5,22,23]. Initially developed for use in the forests of Canada, CFFWIS is composed of six subindexes, namely three fuel moisture codes with a memory component (the Fine Fuel Moisture Code; the Duff Moisture Code; and the Drought Code); two fire behavior indexes based on the aforementioned codes and wind intensity (the Initial Spread Index and the Build-Up Index); and the Fire Weather Index (FWI), which results from the combination of the previous two indexes and is a numeric rating of fire intensity. A complete and thorough description of these indices can be found in Van Wagner [23]. An operational advantage of CFFWIS is that its components solely depend on daily weather observations, usually taken at local noon time, namely air temperature and relative humidity (RH), wind speed, and accumulated daily precipitation. Since the late 1980s and early 1990s, the FWI has been used as a meteorological fire index in a large variety of regions of the world and has proven to be especially suitable for assessing meteorological danger in the Mediterranean basin [5,24–26].

When characterizing plume-dominated wildfires, atmospheric instability is a crucial factor that is not accounted for by the FWI. With the intent of including the effect of atmospheric instability on wildfires, Haines [27] proposed a Lower Atmospheric Severity Index composed of a stability component, which is based on the difference between the absolute temperatures at two prescribed pressure levels chosen based on local surface elevation and a moisture component, corresponding to the lower-level difference between the absolute and dew-point temperatures. The index has since been revised in the form of the so-called Continuous Haines Index (CHI), which has been regularly used in the past decade [28,29]. The CHI requires a dry atmosphere and a steep lapse rate at the lower atmospheric level. If a situation of moist air at a lower level is present, the rising parcel reaches a low lifting condensation level, favorable to the development of storms with heavy rainfall [30]. In a recent study, Pinto et al. [18] proposed an enhanced version of FWI, hereafter FWIe, that explicitly incorporates CHI into the traditional FWI.

To the best of our knowledge, there has been no comprehensive analysis of the relationship between atmospheric instability and wildfire danger indexes. The main goal of this study was to produce a climatological characterization of CHI, FWI, and FWIe over the IP based on state-of-the-art reanalysis ERA5 data provided by the European Centre for Medium-Range Weather Forecasts (ECMWF) [31]. The study then focused on the large fire events that took place in 2003, 2017, and 2018 in Portugal and for each event, the performances of FWI and FWIe were compared. This analysis allowed us to assess the usefulness of FWIe in regions where and during periods when atmospheric instability plays a decisive role in the development of wildfires, contributing to a more efficient deployment of suppression activities.

2. Data and Methods

2.1. Study Region

This study focused on the Iberian Peninsula spanning the period between 1980 and 2020. The regionalization described in Sousa et al. [32] and Trigo et al. [33] was adopted here to divide the area into four clusters (Figure 1) with characteristic normalized burnt area behaviors, namely: a northwestern cluster aggregating the northern half of Portugal and the extreme northwest of Spain (NW), which is the most fire-prone cluster of the

entire study region with large fire activity in August; a southwestern cluster including the southern and interior regions of Portugal and central and southwestern Spain (SW), which is the second most fire-prone cluster in the region, with fire activity mostly prevailing in the summer months; an eastern cluster including the coast and pre-coastal areas east of Gibraltar up to the Pyrenees (E), which presents a higher danger of fire at the beginning of summer; and a northern cluster corresponding to regions over the mountainous sectors of northern Spain, such as the Asturias, Cantabria, and Basque Country (N), which is the least dangerous region with two moderate peaks of fire activity taking place in March and September (Figure 1).

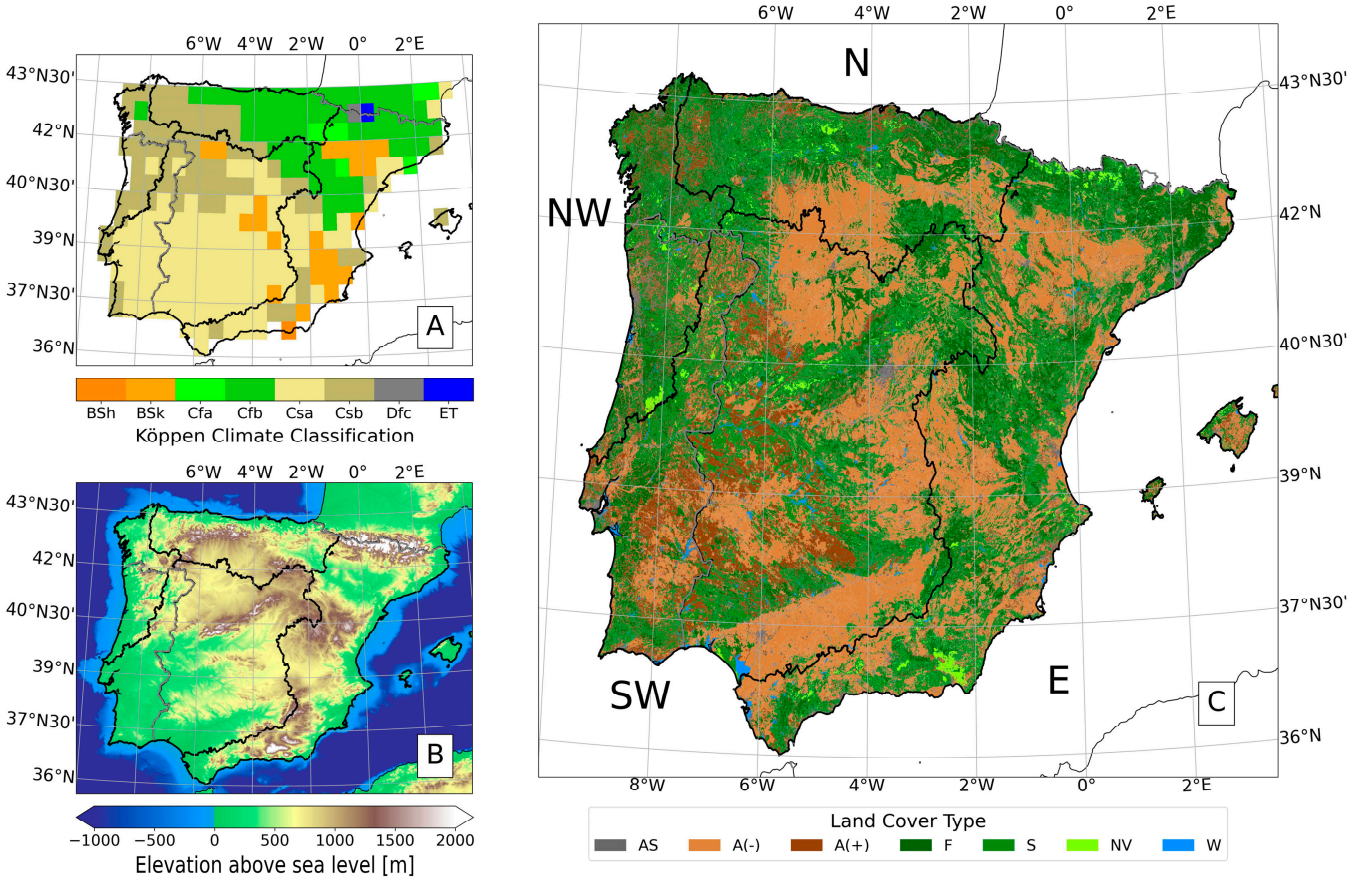

Figure 1. Detailed views of the study region including (**A**) Köppen climate types, as follows: BSh—hot semi-arid, BSk—cold semi-arid, Cfa—humid subtropical, Cfb—temperate oceanic, Csa—hot summer Mediterranean, Csb—warm summer Mediterranean, Dfc—subarctic, Et—tundra; (**B**) topography; and (**C**) land cover types, labeled as follows: AS—artificial surfaces, A(−)—agricultural (less forested), A(+)—agricultural (more forested), F—forest, S—shrub, NV—no vegetation, W—water. In each subplot, the clusters are drawn (in black) as well as the borders (in grey) of Portugal and Spain.

The study region comprised the Iberian Peninsula and is shown in Figure 1, where the Köppen climate types (Figure 1A), topography (Figure 1B), and land cover types (Figure 1C) are also detailed. The Köppen climate types (Figure 1A) for the IP were retrieved from Chen and Chen [34], showing that the IP mainly presents mild, temperate, and dry climate types with dry summers, while the northeastern area is humid all year long. The topography of the study region (Figure 1B) was retrieved from Smith and Sandwell [35], with most of southwestern Iberia being flat and presenting low values of altitude, whereas central, eastern, north, and northeastern Iberia includes large mountain ranges, peaking at nearly 3500 m, with most areas being below 1000 m. Land cover types were retrieved from the Copernicus Land Monitoring Service, CORINE Land Cover (CLC) 2018 [36], derived from satellite imagery obtained at different times during 2017 (e.g., forest types were retrieved

during the July–August period, since this land cover is more developed at this time of the year), with an approximate resolution of 100 m. The spatial distribution of land cover types revealed a close connection to that of the topography, with agricultural cover over much of the mountainous slopes and river valleys of the Peninsula. In the main mountain ranges located in the central and northwestern sectors of the Peninsula, there is a prevalence of forested areas. In central Portugal, a scar of no vegetation is visible, to which the 2017 summer wildfires contributed substantially [37]; however, the October wildfires are not visible due to the time of retrieval for this land cover type (July–August).

2.2. Reanalysis Data

Surface and atmospheric data were retrieved from the 5th generation of the European Centre for Medium-Range Weather Forecasts (ECMWF) global reanalysis (ERA5) [31], available in a $0.25^\circ \times 0.25^\circ$ spatial grid, to calculate CHI, FWI, and FWIe. For the computation of these indexes, we retrieved relative humidity (RH) at 850 hPa, temperature at 2 m and 700 and 850 hPa, the dew-point temperature at 2 m, U and V wind components at 10 m, and accumulated daily precipitation (computed from hourly values). All fields refer to 12 UTC.

2.3. Continuous Haines Index

We elected to use reasonable atmospheric levels to evaluate the CHI considering the average topography of the IP [38]; thus, we chose to use 850–700 hPa. The CHI is defined as:

$$CA = (T_{850} - T_{700})/2 - 2 \quad (1)$$

$$CB = \min(T_{850} - Td_{850}, 30)/3 - 1 \quad (2)$$

$$\text{If } CB > 5, \text{ then: } CB = 5 + (CB - 5)/2$$

$$CHI = CA + CB \quad (3)$$

where T_{700} and T_{850} are the absolute temperature values at 700 and 850 hPa, respectively, and Td_{850} is the dew-point temperature at 850 hPa. The min ($T_{850} - Td_{850}$, 30) term in Equation (2) indicates that an upper bound of 30° C was defined for the difference between the temperature and dew-point temperature at 850 hPa. The dew-point temperature (Td) was computed from T and RH according to the Magnus formula, which yields a conversion between relative humidity and dew-point temperature with a relative error lower than 0.4% over the range $-40\ ^\circ C \leq T \leq 50\ ^\circ C$ [39]. Daily values of the CHI for the IP spanning the study period of 1980–2020 were computed according to relations (1)–(3) using reanalysis data from ERA5.

2.4. Fire Weather Index and Enhanced Fire Weather Index

As with CHI, the FWI system indexes were calculated for the IP spanning the full period using reanalysis data from ERA5. Daily values of the FWI were obtained following the source code of Wang et al. [26], with RH obtained from T and Td using the Magnus formula [39].

In this study, we computed the enhanced FWIe using the code made available by Pinto et al. [18]. This calculation was highly dependent on the region of study and to a lesser degree on the temporal window studied. In the case of higher-than-usual CHI values, i.e., in the case of high atmospheric instability in the lower levels, FWIe presents larger values than FWI; conversely, in the case of a lower-than-usual CHI, the FWIe has lower values relative to the FWI [18].

2.5. Fire Radiative Power

Information about the intensity and severity of fires was based on the power released by the event, which was determined according to the fire radiative power (FRP) using the MODIS Collection 6 Active Fire Product [40] with data availability from 2001 to 2020 (https://earthdata.nasa.gov, last accessed on 11 January 2023). For each fire, the database

provided the local coordinates; date and time; fire confidence; fire radiative power (expressed in megawatts); and type of hotspot (presumed vegetation fire, active volcano, other static land source, or offshore). For this study, we considered the FRP of all events with a fire confidence greater than 90% and classified as presumed vegetation fires.

2.6. Methods

For the 41 years of this study (1980–2020), a series of climatological fields were produced for each variable over the study region for the period spanning from June to September, hereafter referred to as the summer months. Climatologies for the whole year and for an extended period of colder months (November–April) may also be found in the Supplementary Material. Additionally, the intra-annual evolution of each index is presented in the form of boxplots, considering the clusters described in Section 2.1, where the box indicates the interquartile distance, the dash inside the box indicates the median, and the whiskers represent the 5th and 95th percentiles.

Changes in the CHI, FWI, and FWIe in the past four decades were assessed based on the seasonal variability, which was analyzed considering each decade independently. Additionally, we produced the same distributions for each cluster individually. Spatial change was assessed by computing the long-term trend for each of the variables using a monotonic seasonal Mann–Kendall trend test for the summer months. This trend is presented as the average index change per decade, and the non-significant areas (5% significance level) were identified.

The two fire risk indexes were compared with the observed FRPs over the IP, with the objective of comparing risk with occurrences. The FWI and FRP were stratified into predefined classes according to the following criteria: for FWI, the danger class system detailed in EFFIS [41], which presents the indexes in 6 classes ranging from "Very low" to "Extreme" danger; for the FRP, percentile-based classes as defined by percentiles 10, 33, 50, 67, and 90 of the FRP relative to the IP. For each of the FRP classes, a comparison was made between the FWI and FWIe associated with fire events. For this purpose, a linear regression was estimated for each FWI class (totaling 6 equations), the slope of each regression indicating which index had the largest magnitude. Furthermore, for each FRP class, a kernel density estimation (KDE) plot was obtained from the sample using a Gaussian kernel [42]. For both the linear regressions and the KDE plot, the FRP values were used as weights for the computations, i.e., the larger the FRP absolute value, the larger the influence on the result when comparing with other elements in the same set.

Furthermore, we also analyzed case studies: the two fire episodes of June and July 2017, and the two Monchique episodes of 2003 and 2018. The first case, in 2017, was chosen to validate the applied methodology by computing the indexes, as previous studies were available. The fire season of 2017 was exceptional for central and northern Portugal and parts of Galicia, although only the region inside the borders of Portugal and north of the 39.1° N parallel were analyzed in this study; this area encompassed 73% of all occurrences at that time and saw an excess burning of 500,000 ha and the tragic passing of 116 people [37]. Two additional case studies were conducted, wherein, instead of the whole fire season, only consecutive days of significant fires over a small area were analyzed. The fire season of 2003 was outstanding for western Europe and particularly for Portugal [6], with a massive fire that affected the Algarve, in the Monchique region. Years later, in 2018, 80% of this same region that had previously been affected was again subject to a large fire [43]. The choice of the study area in Monchique was motivated by the large mountain range in the area, increasing the interest regarding interactions with atmospheric instability. In all cases, a daily analysis was performed by taking the values of each variable and the respective daily FRP. Besides computing the absolute values of these variables, we also considered their anomalous character using standardized anomalies, i.e., the number of standard deviations above/below the climatological value for the region and the period. Additionally, we also computed the associated probability of exceedance assuming that the distribution of these values was normal.

3. Results

3.1. Climatological Analysis

In the summer months of JJAS, it was possible to identify higher CHI values in the southern part of Iberia, namely in the southeast/central east regions (Figure 2A), with a noticeable band at the 3° W meridian, which roughly corresponded to the junction of the Baetic Mountains, the Central System, and the Iberian System, all visible in the topographic map (Figure 1B). The spatial patterns of the FWI (Figure 2B) showed the largest values located over central Iberia, an area of a typical Mediterranean climate (Figure 1A), with hot to very hot and dry summers. Regions characterized by larger FWI values were typically contained inside the SW and E clusters. Finally, the spatial climatological pattern of the FWIe (Figure 2C) was overall more similar to that of the FWI, as was expected, since these variables were directly related. Nevertheless, the peak of CHI values observed in the border separating the SW and E clusters (Figure 2A) was partially recognizable in the FWIe (Figure 2C) but less evident in the original FWI pattern (Figure 2B). The spatial patterns of the CHI, FWI, and FWIe representing yearly and winter (DJF) climatologies may be found in Supplementary Materials Figure S1A–F, with similar results when considering the yearly patterns and noticeably lower values in winter.

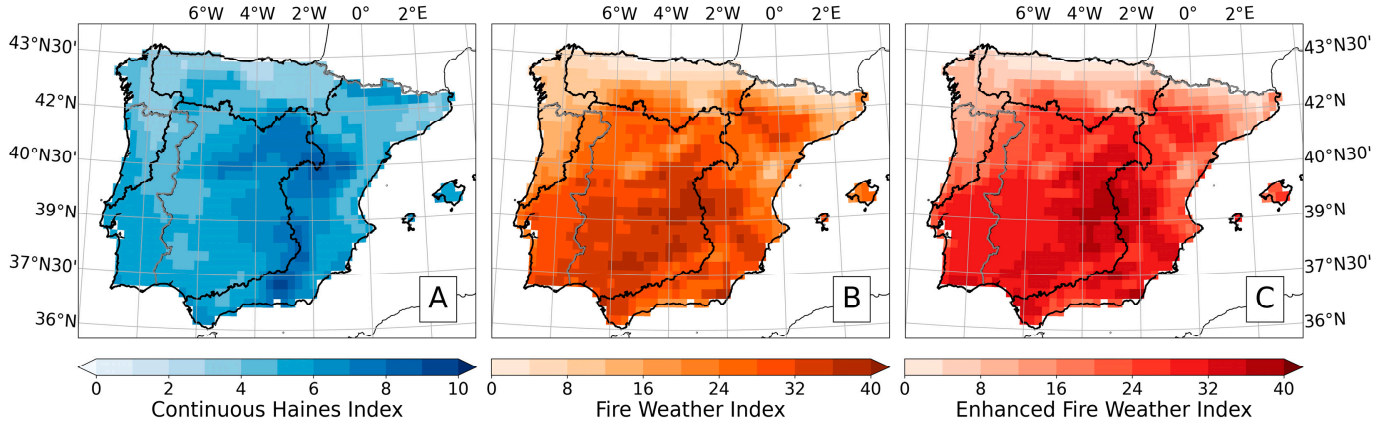

Figure 2. Field climatologies for the Iberian Peninsula for the 1980–2020 period considering the summer months of June, July, August, and September (JJAS) for the three indexes (**A**) CHI, (**B**) FWI, and (**C**) FWIe.

The annual cycle of the three indexes is displayed in the form of monthly boxplots in Figure 3 for each spatial cluster. The annual cycles depended on the region of analysis and were conditioned by the different types of climate, topography, and land cover, as depicted in Figure 1. The CHI distribution had the most notable change from region to region since the seasonal amplitude varied dramatically (Figure 3A–D). The northern part of Iberia, i.e., the NW and N clusters (Figure 3B,C, respectively), comprising the more humid areas of the Peninsula, showed lower overall CHI values (around 3 in winter and nearly 4 in the summer) and a lower yearly amplitude. In turn, the drier and warmer southern and central areas, i.e., the SW and E clusters (Figure 3A,D, respectively), showed the largest amplitude from winter to summer and the largest CHI values, surpassing 6. Additionally, the E cluster (Figure 3D) presented the greatest variability, namely in the warmer months. This higher variability found in the E cluster may have been due to the large meridional extent of the cluster, comprising regions from coastal to inland both in southern Spain and bordering the Pyrenees.

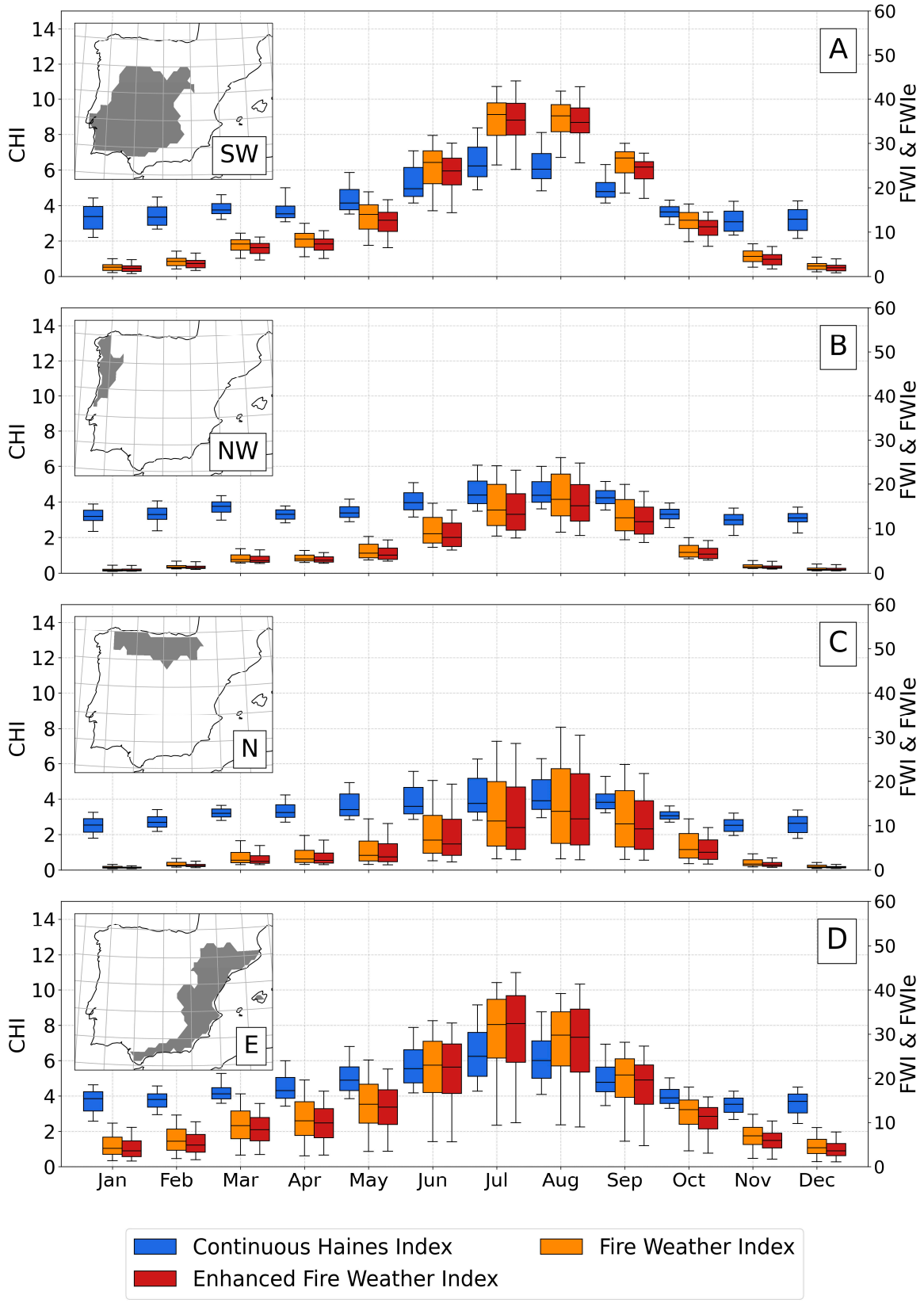

Figure 3. Annual cycles for each of the 4 clusters, (**A**) SW, (**B**) NW, (**C**) N and (**D**) E, during the period 1980–2020 for CHI (blue boxes), FWI (orange boxes), and FWIe (red boxes). The scale for CHI is on the left-hand *y*-axis, and the scale for FWI and FWIe is on the right-hand *y*-axis.

FWI, in comparison with CHI, had a more well-defined seasonality, with higher values and variability in the summer months (Figure 3A–D) and maximum median values around the 35 and 95th percentile maximums reaching 45. The SW cluster (Figure 3A) was characterized by a marked annual cycle in the FWI, with higher values in summer and low variability overall. Moreover, the variability of the FWI in the E region could be explained by its southernmost area sharing the characteristics of the SW cluster (higher FWI values in warmer months), while the northern area had a temperate oceanic climate (Figure 1A), with milder summers and winters (less seasonal temperature variation), contributing to a year-round lower FWI. The NW and N clusters (Figure 3B,C, respectively) had lower FWI scores when compared to the SW and E regions, with median values of 15 and 10, respectively. The NW region has a mostly warm summer Mediterranean climate, and the N region, with its mountainous character due to the presence of the Cantabrian Mountains (Figure 1B), has a mix of the above climate type and a temperate oceanic climate (Figure 1A). The annual cycles of the FWIe (Figure 3A–D) showed similar behavior to those of the FWI across all regions, usually with lower average and spread values, except for July and August in the E region (Figure 3D), where the variability increased overall. It is also noteworthy that different areas within these clusters presented different medians and respective extremes, due to the smaller-scale differences in land cover and climate types.

3.2. Decadal Evolution

Long-term changes were evaluated by performing a decadal evolution assessment of the IP average CHI, FWI, and FWIe values (Figure 4). From the decadal evolution of the CHI (Figure 4A), a similar seasonal cycle to that seen in Figure 3 may be noticed, with median values of around 3 in the colder months and exceeding 6 from June to August. Overall, the months of November, December, and January showed nearly no decadal changes, while from February to April there has been a slight decrease since the 1990s. However, from May to August we observed a general increase since the 1980s, which was also found for September and October since the 1990s (Figure 4A). We performed a similar assessment on a regional basis, and the main conclusions described above for the whole IP were also visible when considering the SW and E regions (Figure S2A and Figure S5A, respectively) and, to a lesser degree, the NW and N regions (Figure S3A and Figure S4A). The spatial distribution of long-term CHI trends is presented in Figure 5A, confirming the identified increments, with the greatest change in the CHI appearing to be mainly located in the southeastern region of the IP, presenting increases of approximately 0.25 and 0.26 per decade in the SW and E regions, respectively (Supplementary Material Table S1 fully describes the changes per decade and statistical significance). The NW and N regions showed smaller increases of about 0.06 and 0.15 per decade, respectively, with only 49% and 66% of their areas presenting statistically significant changes.

The decadal evolution of the IP average FWI and FWIe values (Figure 4B and Figure 4C, respectively) showed similar behaviors to those observed in the seasonal distributions of the SW and E regions (Figure 3A,D). As with the CHI, the colder months (in this case, from November to February) showed no substantial changes in either the FWI or FWIe, while in March and April there was a slight decrease after the 1990s. On the other hand, when considering the summer months, there was a general major increase, namely in May, July, and August. Conversely to the CHI, these increases affected all regions (Figures S2B–S5B and S2C–S5C), with special relevance in the SW and E regions. As with the CHI, the larger trends were located towards the southeast of the Peninsula (Figure 5B,C), with almost the entire IP presenting statistically significant positive trends. Figure 5C shows, for the FWIe, an extended region where the positive trends exceeded four per decade, which resulted from the combined increases in both the CHI and FWI around the same approximated areas. The SW and E regions showed the most relevant changes regarding these decadal trends, with the majority having significant grid boxes with large positive values. Of the SW region's territory, 100% presented statistical significance, and the region showed average increases of approximately 1.9 and 2.2 per decade for the FWI

and FWIe, respectively, while the E region showed slightly lower increases of circa 1.9 and 2.1 for the same variables (Table S1).

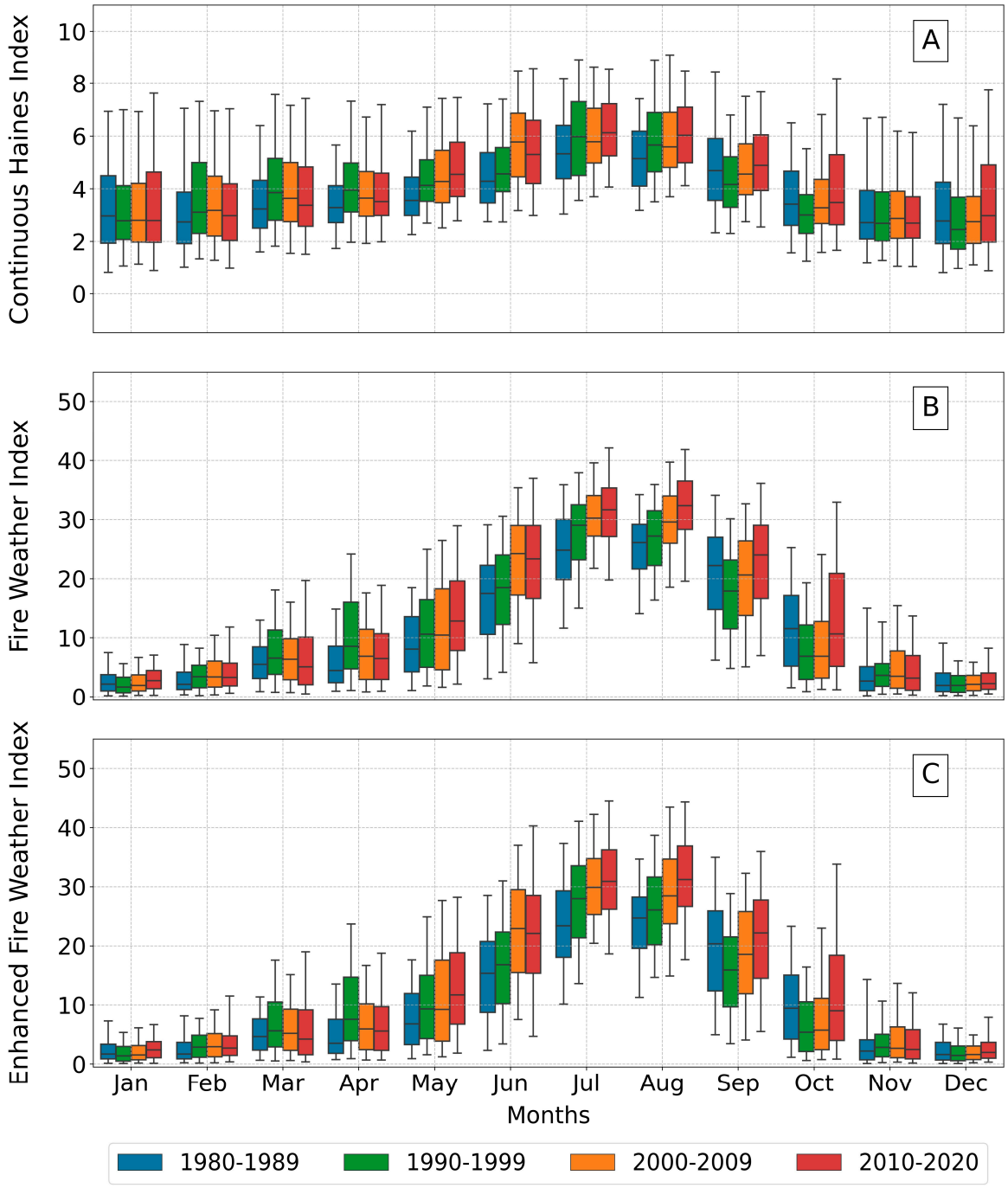

Figure 4. Boxplots showing evolution of the yearly distribution in the IP average throughout the decades of the 1980–2020 period for the variables (**A**) CHI, (**B**) FWI, and (**C**) FWIe.

3.3. Fire Occurrences and FWI vs. FWIe

The relationship with real fire occurrences was examined using FRP as a measure of the power released by each fire observation. We aggregated the computed FRP classes that were defined according to the values of the percentiles 10, 33, 50, 66, and 90 (respectively, 24.9, 53.6, 81.4, 130.1, and 362.3 MW). Each panel of Figure 6 presents the relationship between the FWI and FWIe in two different ways: (1) by means of KDE plots (as shown

by the grey scale) and (2) by means of linear regressions (as shown by the colored lines) estimated for each FWI class (shown as vertical black bars).

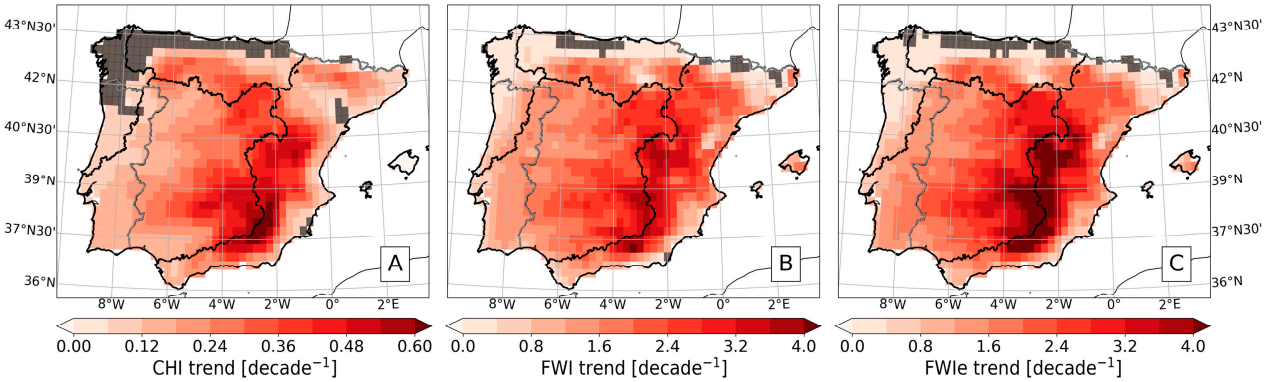

Figure 5. Long-term trends for (**A**) CHI, (**B**) FWI, and (**C**) FWIe, considering only summer months (June to September) for the 1980–2020 period. Computed from a monotonic seasonal Mann–Kendall trend test. Grey shaded areas show pixels where trends were not significant at the 5% statistical level. Trends are shown as the average index change per decade.

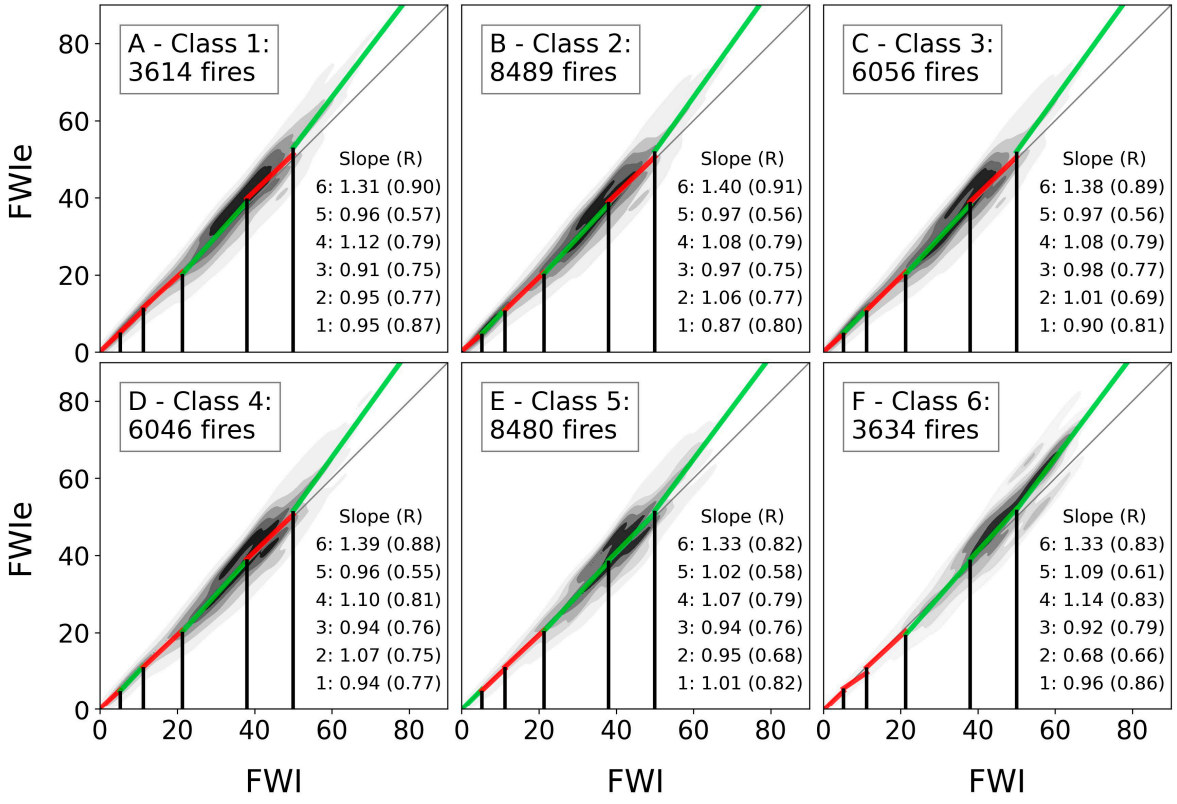

Figure 6. Comparison between real FRP observations (from 2001 to 2020, considering the whole IP) and the FWI and FWIe values for the same occurrences. Both FRP and fire danger indexes were divided into discrete divisions: FRP based on the percentiles 10, 33, 50, 67, and 90 of all occurrences (panels (**A**–**F**), with the respective number of FRPs in that division); and the FWI according to the fire danger classes provided by EFFIS (vertical black lines). The linear regressions for each FWI class compared to FWIe are shown by colored lines: red (green) for slope exceeding (subceeding) the identity line. Values of the slope and associated Pearson R values are shown in each panel, with ascending values (1–6) corresponding to the increasing FWI classes (bottom left to top right within each individual subplot).

It is immediately noticeable from the KDE plot that the bigger the occurrence (i.e., the higher the class of FRP), the more likely it was that an event would happen during more extreme values of the FWI. Fires with an FRP within the first four classes (Figure 6A–D), i.e., with an FRP lower than 130.1, were more likely to coincide with the "high danger" FWI class (up to the fourth vertical black line in Figure 6A–D), with upwards of 35% of these classes' observations falling inside this FWI class. However, fires with FRPs larger than 130.1 corresponded to at most the "very high danger" FWI class (above the fourth vertical black line in Figure 6E,F), also having upwards of 35% representation in this class. It is worth noting that fires with the greatest FRP values (Figure 6F) happened more frequently during the "extreme" than the "high danger" FWI class (30% of the total number of the largest FRP occurrences compared to 25.3%), showing a complete shift in danger associated with the largest fires compared to small-FRP classes.

Looking closely at each FWI class for every panel (colored lines), the linear regression is presented with the associated slope (numerically and in color) and Pearson R value. The first notable detail when comparing the different panels is the FWI classes that preserved the slope type. Firstly, the middle FWI classes ("moderate" and "high", third and fourth, respectively) showed the same behavior in all panels, with the "moderate" ("high") class having a slope below (above) that of the identity line—averaging 0.94 (1.10)—meaning that the FWIe classified the same FRP with a lower (higher) value compared to the FWI. This behavior points to the different nature of the FWIe, which favored a higher danger index for higher FRP values in the upper middle classes. Adding to this, the "extreme" (sixth) FWI class consistently presented higher FWIe values, as seen in all FRP classes, with the highest R values being upwards of 0.83. The reverse could be verified in the "very low" (first) FWI class, with the exception of the fifth (Figure 6E) FRP class. Additionally, the "very high" (fifth) FWI class presented slopes below the identity line in the first four FRP classes (Figure 6A–D), while the last two were above the line (Figure 6E,F); thus, higher (lower) FRP observations were better represented by higher FWIe (FWI) values. To conclude, Figure 6 shows that, overall, higher-FRP occurrences (i.e., more intense fires) tended to logically occur under higher FWI values, and the FWIe generally increased the meteorological danger for these occurrences, while in lower FWI classes, this index maintained greater values compared to the FWIe.

3.4. Case Studies

Figure 7 aggregates the information regarding the CHI, FWI, FWIe, and FRP during the 2017 extended fire season in Portugal, as well as the shapes of all identified burned areas. For the first episode, on June 17th, the CHI reached a value of nearly 10, an extreme value with a probability of exceedance of around 2.5%. This propelled the increase in the FWIe with respect to the FWI, with the latter having a value exceeding 30 and the former reaching 40, which was close to the 2.5% probability of exceedance (Figure 7B). This episode, as evidenced by the grey bars (representing the natural logarithm of the FRP) in Figure 7A, had one of the highest FRP values of this fire season, while the affected area was quite large, as evidenced by Figure 7C (in red). The October 15th episode, towards the end of the extended fire season, showed the maximum recorded FWI values for this region, with a probability of exceedance in the order of 0.005% (Figure 7B). During this episode, as already mentioned, the CHI was also very high, with values resembling those of June (~10, with a probability of exceedance of 2.5%); however, in this instance, the increment observed in the FWIe with respect to the FWI was not so relevant, since the latter was already a record value in itself. This episode led to by far the largest burned area, as seen in Figure 7C (in purple), with several major scars (several larger than 20,000 ha) located all over central and northern Portugal. Comparing both episodes, it became apparent that the June event was more strongly influenced by atmospheric instability, as mentioned in Pinto et al. [37] and depicted in Figure 7, while this contribution was lower in the October episode. These results reinforced the idea that considering the atmospheric instability as

well as the associated meteorological fire danger can provide more insightful information to better characterize extreme events.

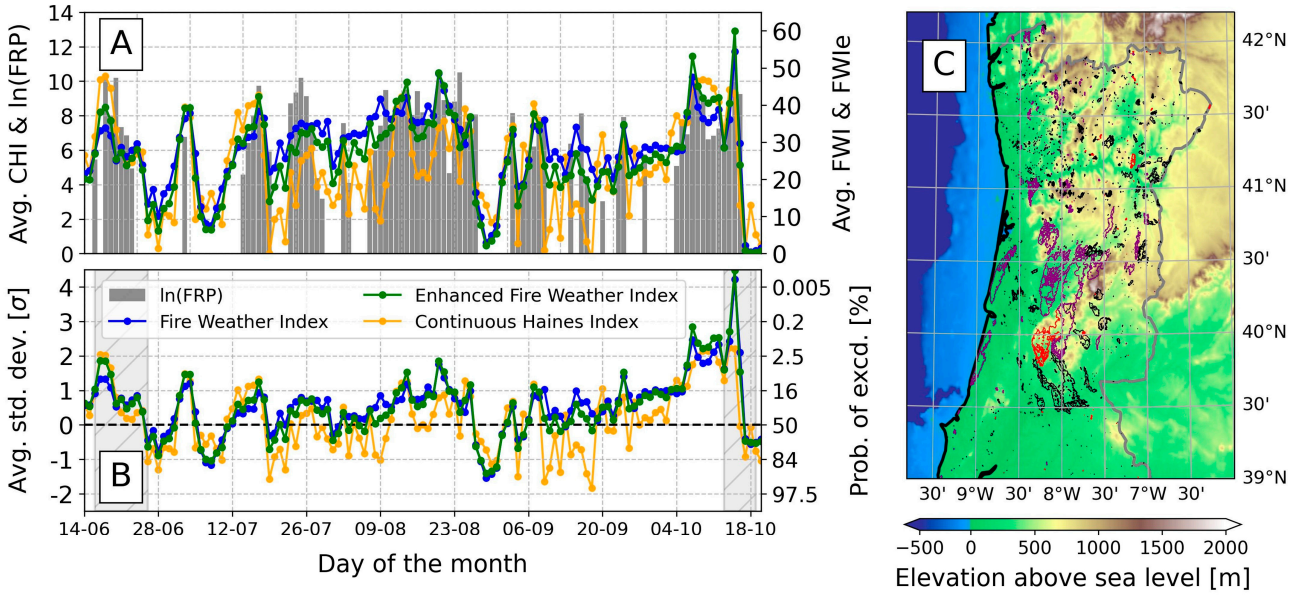

Figure 7. Comparison of the evolution of the CHI (yellow), FWI (blue), and the resulting FWIe (green) during the Portuguese 2017 fire season. (**A**) shows the daily average of each variable spatially averaged over the affected areas in Portugal and the natural logarithm of the daily FRP sum in grey bars. (**B**) shows the exceedance over (or under) the mean value of each variable in the number of standard deviations, and the approximate probability of exceedance can be seen on the right. Shaded grey areas represent the two time periods of the case studies mentioned above and are shown in (**C**) with the respective affected areas in different colors (red for 16−25 June and purple for 13−18 October). More details can be found in the Methods subsection.

The two Monchique study cases considered here are shown in Figure 8. In the top panel (Figure 8A), the location of these events in the southwestern IP region of Algarve, Portugal, is presented. The two-colored outlines denote the two burned areas for 2003 (the larger shape, in purple) and 2018 (the smaller shape, in red). Additionally, the topography of the area, which is presented as a color map, shows that the affected region was mostly mountainous, topping out at roughly 900 m but with several peaks reaching 600 m. This area mostly features a warm summer Mediterranean climate, generally with mild wet winters (Figure 1A), and has a land cover composed mostly of shrubs and forest (Figure 1C). The middle and bottom panels (Figure 8(B1–B3,C1–C3)) show the cases for August 2003 and August 2018, respectively, including the absolute values, the associated excess standard deviation, and the probability of exceedance for all indexes. However, these cases only show the period corresponding to the large fires in the region, depicted in Figure 8(B3,C3) as both the individual FRP observations (scattered dots colored according to the time of occurrence) and the burned area captured in later reports (grey shading; Figure 8(B3) contains regions with no FRP shown inside the shape, since the event occurred later in the season).

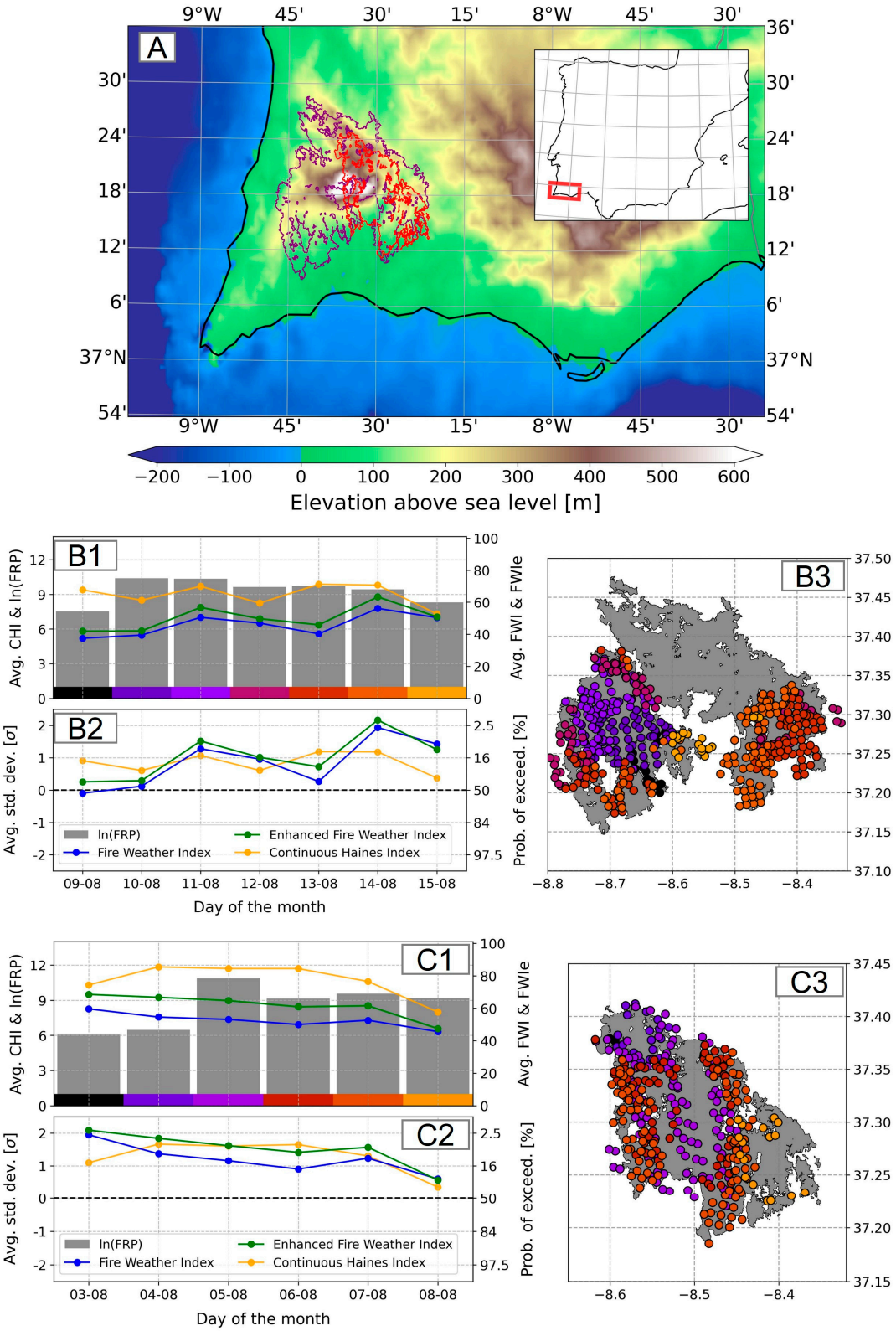

Figure 8. Study case for the Monchique region. Panel (**A**) shows the analyzed area, with the shapes representing the burned areas for 2003 (purple) and 2018 (red); topography is shown by colors. Panels (**B1**–**B3**) and (**C1**–**C3**) show the respective episodes for 2003 and 2018. Subplots 1 and 2 in these panels are as shown in Figure 6, with the addition of the colors corresponding to the day in subplot 3, depicting the affected region and the FRP location via the scattered colored dots.

The August 2003 Monchique study case (Figure 8(B1–B3)) actually comprised two distinct events that occurred close together in time and space. Starting on the 9th of August in the center-right area of the burned shape (Figure 8(B3)), the FWI values were not persistently high on this day over this region, reaching about 38 (Figure 8(B1)) and being close to the mean value (Figure 8(B2)). Atmospheric instability, however, was high, with CHI values above 9 (Figure 8(B1)), nearly one standard deviation above the mean value for this region at this time (Figure 8(B2)). These high CHI values clearly influenced the FWIe to be higher than the FWI; therefore, at this time, the atmospheric instability played a substantial role in increasing the meteorological fire danger FWIe associated with the beginning of this event. As it evolved over the next two days, the FWI increased greatly, while the CHI remained essentially unchanged. During these days, the greatest FRPs were registered (grey bars in Figure 8(B1); note the logarithmic scale), as most of the burned area in Figure 8(B3) was affected. From the 13th of August onwards, a secondary event evolved, eastward of the first one (right side of Figure 8(B3)). At first, the FWI values fell substantially with respect to the previous days, while the CHI was still high, thus increasing the FWIe (Figure 8(B1,B2))—a near copy of the situation on the 9th of August. The following day, the FWI increased to the highest values in this case study, and, with the aid of the still high CHI, the FWIe neared 60, exceeding the two standard deviations over the mean value for this region at that time, with a probability of exceedance below 2.5% (Figure 8(B1,B2)). The last day saw a decrease in the CHI, thus inducing a larger reduction in the FWIe to values identical to those of the FWI, although they were still high; this day coincided with the last FRP observations for this event.

The last study referred to the event that occurred in August 2018, mostly over the area that had already been affected in 2003, as seen in Figure 8A. This case was marked by a high fire meteorological danger, and high FRP values were initially captured on the 3rd of August, with FWI values above 50, which was two standard deviations above the mean value for this region, and a probability of exceedance close to 2.5% (Figure 8(C1,C2)). At the beginning, the CHI was high, with values approaching 11; however, the difference was not substantial between the FWI and FWIe (Figure 8(C1,C2))—similar behavior to that for October 2017 depicted in Figure 7. As the days progressed, the FWI decreased while the CHI increased to more exceptional values (near 12), causing the decrease in the FWIe to be slightly less substantial, and during these days (more specifically, on the 5th of August) the largest FRPs were registered. The last two days of this event saw a decrease in the atmospheric instability, which resulted in the FWIe values approaching those of the FWI.

4. Discussion and Summary

This study comprehensively analyzed the relationship between atmospheric instability and fire risk using the novel FWIe, recently developed by Pinto et al. [18], which associates the well-established instability index known as the Continuous Haines Index (CHI) and the most widely used meteorological fire danger index, the FWI. We extensively studied this relationship over the IP from a climatological viewpoint for the period of 1980 to 2020. Additionally, we considered the observed occurrences of fires according to the FRP from 2001 to 2020 and compared them to several fire danger classes proposed by EFFIS. Finally, we examined several specific case studies to identify the behavior of the new FWIe in relation to the older FWI and checked its success in assessing meteorological fire danger over the Iberian region.

A climatological analysis of the CHI showed that the largest values of this atmospheric instability metric were located mainly in the southern region of Iberia. This may be attributed to the more complex topography of the region—although the northern part of Iberia presents some complex topography, the temperatures are substantially lower, de-creasing the convective instability [44]. The regions that correspond to the junction of the Baetic Mountains, the Central System, and the Iberian System presented the largest values of the CHI in summer, with an absolute maximum in Sierra Nevada. Regarding the FWI and FWIe, the highest values were found in southern regions, which are not

typically fire-prone locations. Indeed, the land cover over these areas is mainly cropland, and the only vegetated areas are in mountainous regions. The most fire-prone regions were those located in northwestern Iberia, namely the north of Portugal and the Spanish northwest region of Galicia [45], which, although showing lower values of the FWI and FWIe, must be considered as critical regions due to a combination of weather/climate, vegetation, geographical, and human factors [33]. Furthermore, the northwestern IP is also a crucial region of rising fire danger for the future, especially in the months of June, July, and August [9]. The values of the FWIe tended to be on average lower than those of the FWI, implying that predominantly stable conditions decreased (albeit slightly) the fire risk level provided by the standard FWI. This may be viewed as an inherent characteristic of the new enhanced FWIe, which favored an increase in the more extreme values to better evaluate the most intense occurrences and downgraded the less dangerous ones [18].

In addition to their seasonal variability, the three indexes significantly increased over the past four decades. These increases were prevalent over the warmer months from May to October, especially affecting the meteorological fire danger indexes (FWI and FWIe), which had major increases in May, July, and August, months belonging to the so-called extended fire season. During these warmer months, most of the IP suffered a significant increase in all three variables, with the exception of the northwestern part of Iberia in the NW and N clusters for the CHI. The SW and E regions were again found to be characterized by the most significant increments in long-term trends. The maximum decadal trends of the FWIe occupied a much larger area compared to those of the FWI; this was expected, since the FWIe incorporated results from the CHI and FWI, which did not present maximum decadal trends that coincided spatially. The specific location of these changes should be further analyzed in future studies focused on local-scale analysis. Moreover, several studies have predicted an increase in fire-danger-associated indexes, namely the FWI, associated with an increase in the mean air temperature in most of this region, related to anthropogenic climate change [1,7–9,32].

Comparing the FWI and FWIe, we found the latter to be useful in differentiating events in which convective meteorological situations helped to enhance the fire risk and eventually fire propagation. This was determined by considering different classes of observed fire occurrences (in the form of FRP values) and comparing these to the fire danger classes proposed by EFFIS. The comparison between the observed FRPs and the calculated FWI and FWIe values allowed us to verify that the higher the FRP class (i.e., the larger the occurrence), the greater the probability of the observations falling into the higher FWI classes. In fact, in the two strongest FRP classes (i.e., above 130.1 MW), the biggest FWI classes (i.e., "high" danger and upwards) presented consistently higher FWIe compared to FWI values. These results led to the conclusion that the FWIe better represented the meteorological fire danger in these extreme cases. Overall, our results showed that higher FRP classes were more prone to be affected by atmospheric instability than lower meteorological fire danger situations. Moreover, for most of the six FRP classes considered, the reverse was also found (despite some marginal exceptions), with lower danger classes (i.e., "moderate" danger and below) presenting a higher FWI compared to FWIe value. To conclude, we can state that higher FRP values (i.e., more intense fires) tended to occur in concert with higher FWI values, and the FWIe generally increased the meteorological danger for these occurrences; conversely, for lower FWI classes, this index maintained greater values compared to the FWIe.

The two case studies of the 2017 Portuguese fire season, which took place on the 17th of June and on the 15th of October, were thoroughly compared [37]. The results showed that the June episode presented larger convective circulation, which helped to propel the fire intensity, i.e., the CHI was higher, and therefore the fire risk was much higher. On the other hand, the October episode included the aggravating passage of Hurricane Ophelia (2017) just west of the Iberian coast, which, despite not directly increasing the convective circulation over the region, increased the wind intensities observed in these areas, which in turn induced increased CHI values. Overall, despite their very different nature and impacts, both extreme fire episodes in 2017 included a high convective potential for fire

spreading, although this mechanism was more relevant for the June episodes according to [37].

Finally, we evaluated the role of the CHI, FWI, and FWIe for the case studies of the Monchique megafires that occurred in the 2003 and 2018 fire seasons in southwestern IP. The 2003 event covered two August fires, the first started on the 8th at Marmelete and the second initiated on the 12th at Silves. At the beginning of both occurrences, atmospheric instability was found to be significant in enhancing the meteorological fire danger in the form of the FWIe, while at the very end of the episodes the reverse was observed, and the value of the FWIe fell below that of the FWI. In 2018, the event also took place in August, starting on the 3rd near the town of Monchique; 80% of the area affected by this fire had already been burned by the previous fires from 2003. In this case, the FWI presented high values throughout the event, though with a small decrease and high atmospheric instability at the beginning. As the event progressed, the instability increased, attenuating the decrease observed in the FWI during the days with the greatest FRPs. At the end of the event, both the instability and the meteorological fire danger decreased substantially, encouraging the end of the event. These case studies both affected the same general area (the slopes of the Monchique Range), 15 years apart. As previously mentioned, the CHI was observed to be higher in places of topographic complexity, and, as these case studies made clear, the atmospheric instability (that was already high in these places) showed exceptional values above 10 (reaching 12 in 2018). Previous studies have pointed out that extreme CHI values above 10 imply that it is extremely complex to extinguish fires, and there is an aggravated risk of under-predicted fire behavior [29]. These facts combined indicate that atmospheric instability played an important role in both events.

5. Final Remarks

This study was performed in the framework of the National Roadmap for Adaptation XXI—Portuguese Territorial Climate Change Vulnerability Assessment for XXI Century (RNA2100) project, which is currently being developed with the aim of supporting public policy exercises related to adaptation to climate change. This work aimed to contribute to the development and assessment of a state-of-the-art meteorological fire risk index, the FWIe, which was designed to improve the traditional FWI by incorporating explicitly in its formulation the role played by atmospheric instability. This new enhanced index may represent an important tool, contributing to the forest and wildfire sector's decision-makers, since atmospheric instability is known to play a crucial role in the development of some large wildfires. Indeed, this was the case in the deadly wildfires that occurred in Portugal in June 2017, as shown by the case study analyzed in this paper. Additionally, from a more structural perspective, this work aimed at assessing the FWIe using reanalyzed ERA5 data and paves the way for the development of storylines focused on destructive wildfire events in a climate change context, contributing to the development of timely adaptation strategies. This work overall highlighted the great importance of atmospheric instability in the development of extreme-fire-risk events, providing essential evidence to improve early warning systems in certain places to prevent large catastrophes from happening, such as the increased effectiveness of the FWIe to predict more or less extreme danger situations compared to the more well-established FWI. Future developments in this area are therefore recommended, both locally, regarding potential links with land cover and geographical features such as river basins, near-shore locations, or mountainous areas, and on a policy level, with better territorial planning and vegetation management.

Supplementary Materials: The following supporting information can be downloaded at: https://www.mdpi.com/article/10.3390/fire6030120/s1, Figure S1: Yearly and winter field climatology for the Iberian Peninsula, Figure S2: Decadal evolution of the yearly distribution in the SW cluster for the three variables CHI (A), FWI (B), and FWIe (C), Figure S3: Same as Figure S2 but for the NW cluster, Figure S4: Same as Figure S2 but for the N cluster, Figure S5: Same as Figure S2 but for the E cluster, Table S1: Average geographical trend in each cluster for all three variables.

Author Contributions: L.C.S. and M.M.L.: conceptualization; methodology; software; validation; formal analysis; investigation; data curation; writing (original draft preparation, review, and editing); and visualization. V.A.B. and S.A.N.: validation, formal analysis, investigation, data curation, writing (review and editing), and supervision. C.C.D., A.R., P.M.M.S. and R.M.T.: validation, writing (review and editing), and supervision. R.M.T.: project administration. All authors have read and agreed to the published version of the manuscript.

Funding: This work was funded by EEA-Financial Mechanism 2014–2021 and the Portuguese Environment Agency through Pre-defined Project-2 National Roadmap for Adaptation XXI (PDP-2) and the project "Forecasting fire probability and characteristic for a habitable pyro environment (Fire-Cast)" under grant no. PCIF/GRF/0204/2017, and by the Portuguese Fundação para a Ciência e a Tecnologia (FCT) I.P./MCTES through national funds (PIDDAC)—UIDB/50019/2020.

Institutional Review Board Statement: Not applicable.

Informed Consent Statement: Not applicable.

Data Availability Statement: ERA5 hourly data may be found at https://www.ecmwf.int/en/forecasts/datasets/reanalysis-datasets/era5, last accessed on 11 January 2023. Corine Land Cover was retrieved from https://land.copernicus.eu/, last accessed on 11 January 2023. MODIS FRP was downloaded from https://earthdata.nasa.gov, last accessed on 11 January 2023. Burned area scars were extracted from https://www.icnf.pt/, last accessed on 11 January 2023. All the code used to process the data is available upon request without undue reservation.

Acknowledgments: L.C.S. would like to acknowledge the financial support of FCT through the project "Forecasting fire probability and characteristics for a habitable pyroenvironment (Fire-Cast)" under grant no. PCIF/GRF/0204/2017. M.M.L. would like to acknowledge the project "Extração de dados por chamada de url com parâmetros—CEASEFIRE", financed by E-REDES. V.A.B. is funded by the Pre-defined Project-2 National Roadmap for Adaptation XXI (PDP-2).

Conflicts of Interest: The authors declare no conflict of interest.

References

1. Amatulli, G.; Camia, A.; San-Miguel-Ayanz, J. Estimating future burned areas under changing climate in the EU-Mediterranean countries. *Sci. Total Environ.* **2013**, *450*, 209–222. [CrossRef] [PubMed]
2. Amraoui, M.; Pereira, M.G.; DaCamara, C.C.; Calado, T.J. Atmospheric conditions associated with extreme fire activity in the Western Mediterranean region. *Sci. Total Environ.* **2015**, *524*, 32–39. [CrossRef] [PubMed]
3. Fernandes, P.M.; Monteiro-Henriques, T.; Guiomar, N.; Loureiro, C.; Barros, A.M. Bottom-up variables govern large-fire size in Portugal. *Ecosystems* **2016**, *19*, 1362–1375. [CrossRef]
4. Carmo, M.; Ferreira, J.; Mendes, M.; Silva, Á.; Silva, P.; Alves, D.; Reis, L.; Novo, I.; Viegas, D.X. The climatology of extreme wildfires in Portugal, 1980–2018: Contributions to forecasting and preparedness. *Int. J. Climatol.* **2021**, *42*, 3123–3146. [CrossRef]
5. DaCamara, C.C.; Calado, T.J.; Ermida, S.L.; Trigo, I.F.; Amraoui, M.; Turkman, K.F. Calibration of the fire weather index over mediterranean europe based on fire activity retrieved from msg satellite imagery. *Int. J. Wildland Fire* **2014**, *23*, 945–958. [CrossRef]
6. Trigo, R.M.; Pereira, J.M.; Pereira, M.G.; Mota, B.; Calado, T.J.; Dacamara, C.C.; Santo, F.E. Atmospheric conditions associated with the exceptional fire season of 2003 in Portugal. *Int. J. Climatol.* **2006**, *26*, 1741–1757. [CrossRef]
7. Abatzoglou, J.T.; Williams, A.P.; Barbero, R. Global emergence of anthropogenic climate change in fire weather indices. *Geophys. Res. Lett.* **2019**, *46*, 326–336. [CrossRef]
8. Bedia, J.; Herrera, S.; Camia, A.; Moreno, J.M.; Gutiérrez, J.M. Forest fire danger projections in the Mediterranean using ENSEMBLES regional climate change scenarios. *Clim. Change* **2014**, *122*, 185–199. [CrossRef]
9. Calheiros, T.; Nunes, J.P.; Pereira, M.G. Recent evolution of spatial and temporal patterns of burnt areas and fire weather risk in the Iberian Peninsula. *Agric. Forest Meteorol.* **2020**, *287*, 107923. [CrossRef]
10. Pereira, M.G.; Calado, T.J.; DaCamara, C.C.; Calheiros, T. Effects of regional climate change on rural fires in Portugal. *Clim. Res.* **2013**, *57*, 187–200. [CrossRef]
11. Lionello, P.; Malanotte-Rizzoli, P.; Boscolo, R.; Alpert, P.; Artale, V.; Li, L.; Luterbacher, J.; May, W.; Trigo, R.; Tsimplis, M.; et al. The Mediterranean climate: An overview of the main characteristics and issues. *Dev. Earth Environ. Sci.* **2006**, *4*, 1–26. [CrossRef]
12. Nunes, S.A.; DaCamara, C.C.; Turkman, K.F.; Calado, T.J.; Trigo, R.M.; Turkman, M.A. Wildland fire potential outlooks for Portugal using meteorological indices of fire danger. *Nat. Hazard. Earth Sys.* **2019**, *19*, 1459–1470. [CrossRef]
13. San-Miguel-Ayanz, J.; Durrant, T.; Boca, R.; Maianti, P.; Libertá, G.; Artés Vivancos, T.; Jacome Felix Oom, D.; Branco, A.; De Rigo, D.; Ferrari, D.; et al. *Forest Fires in Europe, Middle East and North Africa 2020*; Publications Office of the European Union: Luxembourg, 2021. [CrossRef]

14. Leone, V.; Lovreglio, R.; Martín, M.P.; Martínez, J.; Vilar, L. Human factors of fire occurrence in the Mediterranean. In *Earth Observation of Wildland Fires in Mediterranean Ecosystems*, 1st ed.; Springer: Berlin, Germany, 2009; pp. 149–170. [CrossRef]
15. Gómez-González, S.; Ojeda, F.; Fernandes, P.M. Portugal and Chile: Longing for sustainable forestry while rising from the ashes. *Environ. Sci. Policy* **2018**, *81*, 104–107. [CrossRef]
16. Alcubierre, P.C.; Ribau, M.C.; de Egileor, A.L.O.; Bover, M.M.; Kraus, P.D. *Prevention of Large Wildfires Using the Fire Types Concept*; Unitat Técnica del GRAF: Barcelona, Spain, 2011.
17. Lecina-Diaz, J.; Alvarez, A.; Retana, J. Extreme fire severity patterns in topographic, convective and wind-driven historical wildfires of Mediterranean pine forests. *PLoS ONE* **2014**, *9*, e85127. [CrossRef] [PubMed]
18. Pinto, M.M.; DaCamara, C.C.; Hurduc, A.; Trigo, R.M.; Trigo, I.F. Enhancing the fire weather index with atmospheric instability information. *Environ. Res. Lett.* **2020**, *15*, 0940b7. [CrossRef]
19. Ruffault, J.; Moron, V.; Trigo, R.M.; Curt, T. Daily synoptic conditions associated with large fire occurrence in Mediterranean France: Evidence for a wind-driven fire regime. *Int. J. Climatol.* **2017**, *37*, 524–533. [CrossRef]
20. Flatley, W.T.; Lafon, C.W.; Grissino-Mayer, H.D. Climatic and topographic controls on patterns of fire in the southern and central Appalachian Mountains, USA. *Landsc. Ecol.* **2011**, *26*, 195–209. [CrossRef]
21. Lareau, N.P.; Clements, C.B. The mean and turbulent properties of a wildfire convective plume. *J. Appl. Meteorol. Clim.* **2017**, *56*, 2289–2299. [CrossRef]
22. Jolly, W.M.; Freeborn, P.H.; Page, W.G.; Butler, B.W. Severe fire danger index: A forecastable metric to inform firefighter and community wildfire risk management. *Fire J.* **2019**, *2*, 47. [CrossRef]
23. Van Wagner, C. *Development and Structure of the Canadian Forest Fire Weather Index System*; Can. For. Serv., Forestry Tech. Rep.: Ottawa, Canada, 1987.
24. Karali, A.; Roussos, A.; Giannakopoulos, C.; Hatzaki, M.; Xanthopoulos, G.; Kaoukis, K. Evaluation of the Canadian Fire Weather Index in Greece and future climate projections. In *Advances in Meteorology*; Springer: Berlin/Heidelberg, Germany, 2013; pp. 501–508. [CrossRef]
25. Pinto, M.M.; DaCamara, C.C.; Trigo, I.F.; Trigo, R.M.; Turkman, K.F. Fire danger rating over mediterranean europe based on fire radiative power derived from meteosat. *Nat. Hazard Earth Sys.* **2018**, *18*, 515–529. [CrossRef]
26. Wang, Y.; Anderson, K.R.; Suddaby, R.M. Updated source code for calculating fire danger indices in the Canadian Forest Fire Weather Index System. In *Canadian Forest Service, Northern Forestry Centre Information Rep, Natural Resources Canada*; NOR-X-424: Edmonton, Canada, 2015; p. 26. Available online: https://cfs.nrcan.gc.ca/publications (accessed on 11 March 2022).
27. Haines, D.A. A lower atmospheric severity index for wildland fires. *Natl. Weather. Dig.* **1988**, *13*, 23–27.
28. Dowdy, A.J.; Pepler, A. Pyroconvection risk in Australia: Climatological changes in atmospheric stability and surface fire weather conditions. *Geophys. Res. Lett.* **2018**, *45*, 2005–2013. [CrossRef]
29. Mills, G.A.; McCaw, L. *Atmospheric Stability Environments and Fire Weather in Australia—Extending the Haines Index*; Technical Report; Centre for Australian Weather and Climate Research: Victoria, Australia, 2010; Volume 20.
30. Stull, R.B. *An Introduction to Boundary Layer Meteorology*; Springer: Berlin/Heidelberg, Germany, 1988; Volume 13.
31. Hersbach, H.; Bell, B.; Berrisford, P.; Hirahara, S.; Horányi, A.; Muñoz-Sabater, J.; Nicolas, J.; Peubey, C.; Radu, R.; Schepers, D.; et al. The era5 global reanalysis. *Q. J. R. Meteor. Soc.* **2020**, *146*, 1999–2049. [CrossRef]
32. Sousa, P.M.; Trigo, R.M.; Pereira, M.G.; Bedia, J.; Gutiérrez, J.M. Different approaches to model future burnt area in the Iberian Peninsula. *Agric. Forest Meteorol.* **2015**, *202*, 11–25. [CrossRef]
33. Trigo, R.M.; Sousa, P.M.; Pereira, M.G.; Rasilla, D.; Gouveia, C.M. Modelling wildfire activity in Iberia with different atmospheric circulation weather types. *Int. J. Climatol.* **2016**, *36*, 2761–2778. [CrossRef]
34. Chen, D.; Chen, H.W. Using the Köppen classification to quantify climate variation and change: An example for 1901–2010. *Environ. Dev.* **2013**, *6*, 69–79. [CrossRef]
35. Smith, W.H.; Sandwell, D.T. Global sea floor topography from satellite altimetry and ship depth soundings. *Science* **1997**, *277*, 1956–1962. [CrossRef]
36. Büttner, G.; Kosztra, B.; Kleeschulte, S.; Hazeu, G.; Vittek, M.; Schroder, C.; Littkopf, A. *Copernicus Land Monitoring Service: Corine Land Cover*; EEA: Copenhagen, Denmark, 2021.
37. Pinto, M.M.; Hurduc, A.; Trigo, R.M.; Trigo, I.F.; DaCamara, C.C. The extreme weather conditions behind the destructive fires of June and October 2017 in Portugal. In *Advances in Forest Fire Research*; University of Coimbra: Coimbra, Portugal, 2018. [CrossRef]
38. Winkler, J.A.; Potter, B.E.; Wilhelm, D.F.; Shadbolt, R.P.; Piromsopa, K.; Bian, X. Climatological and statistical characteristics of the Haines Index for North America. *Int. J. Wildland Fire* **2007**, *16*, 139–152. [CrossRef]
39. Lawrence, M.G. The relationship between relative humidity and the dewpoint temperature in moist air: A simple conversion and applications. *B. Am. Meteorol. Soc.* **2005**, *86*, 225–234. [CrossRef]
40. Giglio, L.; Schroeder, W.; Hall, J.V.; Justice, C.O. *MODIS Collection 6 Active Fire Product User's Guide Revision B*; Department of Geographical Sciences, University of Maryland: College Park, MD, USA, 2018.
41. European Forest Fire Information System (EFFIS). "Fire Danger Forecast". Available online: https://effis.jrc.ec.europa.eu/about-effis/technical-background/fire-danger-forecast (accessed on 11 March 2022).
42. Fotheringham, A.S.; Brunsdon, C.; Charlton, M. *Quantitative Geography: Perspectives on Spatial Data Analysis*, 1st ed.; Sage: London, UK, 2000; p. 288.

43. Rego, F.C.; Fernandes, P.; Sande Silva, J.; Azevedo, J.; Moura, J.M.; Oliveira, E.; Cortes, R.; Viegas, D.X.; Caldeira, D.; Duarte Santos, F. *Avaliação do Incêndio de Monchique. Relatório Observatório Técnico Independente, Comissão Técnica Independente*; Assembleia da República: Lisboa, Portugal, 2019; p. 78.
44. Cunha, S.; Silva, Á.; Herráez, C.; Pires, V.; Chazarra, A.; Mestre, A.; Nunes, L.; Mendes, M.; Neto, J.; Marques, J.; et al. *Atlas Climático Ibérico—Iberian Climate Atlas*; AEMET, Ministerio de Medio Ambiente y Medio Rural y Marino: Madrid, Spain, 2011; p. 80.
45. Rodrigues, M.; Trigo, R.M.; Vega-García, C.; Cardil, A. Identifying large fire weather typologies in the Iberian Peninsula. *Agr. Forest Meteorol.* **2020**, *280*, 107789. [CrossRef]